Mon. Not. R. Astron. Soc. **000**, 1–21 (2007)   Printed 1 February 2008   (MN LaTeX style file v2.2)

arXiv:0707.0717v1 [astro-ph] 5 Jul 2007

Temperature and abundance profiles of hot gas in galaxy groups – I. Results and statistical analysis

Jesper Rasmussen* and Trevor J. Ponman
School of Physics and Astronomy, University of Birmingham, Edgbaston, Birmingham B15 2TT

ABSTRACT
The distribution of metals in groups of galaxies holds important information about the chemical enrichment history of the Universe. Here we present radial profiles of temperature and the abundance of iron and silicon of the hot intragroup medium for a sample of 15 nearby groups of galaxies observed by *Chandra*, selected for their regular X-ray morphology. All but one group display a cool core, the size of which is found to correlate with the mean temperature of the group derived outside this core. When scaled to this mean temperature, the temperature profiles are remarkably similar, being analogous to those of more massive clusters at large radii but significantly flatter inwards of the temperature peak. The Fe abundance generally shows a central excess followed by a radial decline, reaching a typical value of 0.1 Z$_\odot$ within r_{500}, a factor of two lower than corresponding results for clusters. Si shows less systematic radial variation, on average displaying a less pronounced decline than Fe and showing evidence for a flattening at large radii. Off-centre abundance peaks are seen both for Fe and Si in a number of groups with well-resolved cores. Derived abundance ratios indicate that supernovae type Ia are responsible for 80 per cent of the Fe in the group core, but the type II contribution increases with radius and completely dominates at r_{500}. We present fitting formulae for the radial dependence of temperature and abundances, to facilitate comparison to results of numerical simulations of group formation and evolution. In a companion paper, we discuss the implications of these results for feedback and enrichment in galaxy groups.

Key words: galaxies: clusters: general — (galaxies:) intergalactic medium — X-rays: galaxies: clusters

1 INTRODUCTION

Hot X-ray emitting gas constitutes the dominant baryonic component in groups and clusters of galaxies. The metals in this intracluster medium (ICM) are believed to originate mainly in material ejected from group and cluster galaxies by supernovae (Arnaud et al. 1992), with a smaller portion driven out by galaxies through galaxy–galaxy and galaxy–ICM interactions (Domainko et al. 2006, but see also Moll et al. 2007). Besides galactic stellar winds, other non-gravitational processes have also played a role in redistributing the enriched gas, and more generally, in shaping the thermodynamic properties of the ICM. These processes include radiative cooling (Sanderson, Ponman & O'Sullivan 2006), and heating and mixing of gas by active galactic nuclei (Croston, Hardcastle & Birkinshaw 2005; McNamara et al. 2005; O'Sullivan, Vrtilek & Kempner 2005; Rebusco et al. 2006; Roediger et al. 2007). The spatial distribution of metals, and to some extent the temperature structure of the ICM, reflect the action of such processes, thus offering insight into the importance and nature of the mechanisms, other than gravity, that have established the properties of the ICM at the present epoch. Groups of galaxies are particularly interesting in this context because such processes are expected to be relatively more important in low-mass systems due to their shallower gravitational potentials.

Iron and silicon comprise the major diagnostic elements for studies of the ICM abundance distribution, as these elements give rise to the most prominent lines in the soft X-ray spectrum of thermal plasmas, and are among the elements for which there is a distinctively different yield in type Ia and type II supernova explosions according to standard supernova (SN) models (see, e.g., Baumgartner et al. 2005 and references therein). Whilst iron is predominantly produced by SN Ia, silicon is more evenly mixed between the two SN types. The ratio of Si to Fe abundance therefore provides valuable information on the relative importance of SN Ia vs. SN II in enriching the ICM.

Abundance and temperature profiles of massive clusters have received considerable attention (e.g., De Grandi & Molendi 2001; Baumgartner et al. 2005; Vikhlinin et al. 2005; Piffaretti et al. 2005; Donahue et al. 2006). It is now well established that clusters with cool central regions typically exhibit high central Fe abundances (e.g., De Grandi & Molendi 2001; Irwin & Bregman 2001; De Grandi et al. 2004) which can be attributed predominantly to SN Ia enrichment by the stellar population of the central bright cluster galaxy (Finoguenov, David & Ponman 2000;

---

* E-mail: jesper@star.sr.bham.ac.uk

Böhringer et al. 2004; De Grandi et al. 2004). Clusters with no evidence for strong central cooling tend to display a more uniform Fe distribution.

At large radii ($r \gtrsim 0.5 r_{200}$, where r_{200} is the radius enclosing a mean density of 200 times the critical density), $Z_{\rm Fe}$ typically drops to a value ~ 0.2 $Z_\odot$ (Finoguenov et al. 2000; De Grandi & Molendi 2001; Tamura et al. 2004; De Grandi et al. 2004). As suggested by, for example, Finoguenov et al. (2000), this could result from SN II–dominated enrichment at an early stage in the cluster formation via energetic starburst winds. Such a picture receives support from the observation that a substantial fraction of the ICM metals were already in place by $z \sim 1$ (Tozzi et al. 2003; Balestra et al. 2007).

The situation in lower-mass systems is much less clear, despite their relatively larger importance for the cosmic baryon and metal budgets. Historically, this has reflected the difficulty in assembling large samples of groups bright enough to allow detailed, spatially resolved X-ray spectroscopy. Earlier works based on *ROSAT* and *ASCA* data typically featured only a handful of $kT \lesssim 2$ keV groups, often included as part of larger cluster-dominated samples (e.g. Fukazawa et al. 1998; Finoguenov & Ponman 1999; Finoguenov et al. 2000; Finoguenov, Arnaud & David 2001a). Such studies suggested a $Z_{\rm Si}/Z_{\rm Fe}$ ratio roughly solar in groups (Fukazawa et al. 1996, 1998; Davis, Mulchaey & Mushotzky 1999; Hwang et al. 1999), about half the value found in early cluster studies (Mushotzky et al. 1996), with an indication that Si/Fe rises above the solar ratio outside group cores (e.g. Fukazawa et al. 1998; Finoguenov & Ponman 1999). However, the sensitivity and spatial resolution of *ROSAT* and *ASCA* imposed natural limits to the amount of detail one could obtain on the spatial variation of Fe and Si and hence the relative importance of the two supernova types at different group radii (Finoguenov et al. 2002). For the same reasons, it is possible that the so-called Fe and Si biases (Buote 2000a) may have affected some of these earlier results, at least for groups with thermally complex core regions.

With the current generation of X-ray telescopes, the situation has improved dramatically. Recent *XMM* observations have shown that temperature profiles of cool-core groups display a striking similarity and typically peak at a radius $r \sim 0.05 r_{100}$ (Gastaldello et al. 2005), which corresponds to $r \sim 0.1 r_{500}$ for the mass profiles derived for these groups. Another recent study, also based on *XMM* observations, is the work of Finoguenov et al. (2007), who investigated the distribution of temperature, density, metal abundance, and derived quantities using 2-D spectral mapping of a sample of 14 groups. This work showed that, as for clusters, central metal excesses are present in groups with a cool core, a result already hinted at in earlier *ASCA* studies (Buote 2000a).

While *Chandra* lacks the sensitivity of *XMM-Newton*, it has a superior spatial resolution, enabling a more robust removal of point sources, and also experiences a lower and more stable instrumental background. *Chandra* data can therefore complement *XMM* observations of groups, particularly in the group cores, but can also serve as an important validity check on *XMM* results for the X-ray faint outskirts of groups due to the lower background. Here we utilize this to derive radial profiles of temperature and the abundance of Fe and Si from *Chandra* observations of a sample of 15 groups. Particular emphasis is given to combining the results obtained for individual groups to explore statistical trends within the sample. One purpose of doing so is to obtain a clearer picture of the content and behaviour of metals in group outskirts, where most of the intragroup gas resides but where the low X-ray surface brightness often prohibits robust constraints for individual systems. In addition, this approach allows an investigation into the signatures of feedback in group gas, including the origin of metals in SN and the redistribution of gas by active galactic nuclei (AGN), in more detail than is possible on a group-by-group basis. Furthermore, many numerical simulations of groups and clusters now include chemical evolution of the ICM through the actions of galactic starburst winds (e.g., Tornatore et al. 2004; Romeo et al. 2006; Cora 2006), AGN outflows (Moll et al. 2007), and galaxy–ICM interactions (Domainko et al. 2006). Therefore, it also seems timely to provide a firm observational baseline against which to test the input physics in such simulations, from the perspective of their predictions for the chemical (and thermal) properties of the ICM in the group regime.

The paper is structured as follows. In Section 2 we describe the group sample and data analysis procedure, and Section 3 presents the main results for each group. Section 4 discusses the impact of systematic errors on our results. In Section 5 we stack the results for individual groups, to investigate and quantify systematic trends across the sample. Section 6 summarizes the results and presents our conclusions. In a companion paper (Rasmussen & Ponman, in prep.; hereafter Paper II), we discuss the implications of these results for the history and nature of galactic feedback and chemical enrichment within the sample. $H_0 = 70$ km s^{-1} Mpc^{-1} is assumed throughout, and all errors are given at the 68 per cent confidence level unless otherwise stated.

2 GROUP SAMPLE AND DATA ANALYSIS

2.1 Sample selection and data preparation

Our sample is predominantly based on the 25 GEMS groups from the 'G'-sample of Osmond & Ponman (2004). This subsample comprises those GEMS groups that display group-scale X-ray emission (spatial extent of $r \gtrsim 60$ kpc), distinguished this way from systems that remain X-ray undetected and those in which the diffuse emission can be associated with the central galaxy rather than with the group as a whole. From these 25 groups, we effectively imposed a flux limit on the sample by only selecting systems with available *Chandra* archival data containing more than 6,000 ACIS net counts from diffuse emission. This was done in order to enable robust, spatially resolved spectroscopy in a number of regions for each group. In addition, only groups more distant than 20 Mpc were included, to ensure that data extended well outside the central group galaxy. As one of our aims is to investigate signatures of galactic feedback in group gas, and since we wish to study the radial distributions of gas properties, this study requires systems which appear reasonably undisturbed by recent merger activity and associated gas mixing. We therefore also excluded NGC 5171 from the sample, an obviously unrelaxed system already studied in detail by Osmond, Ponman & Finoguenov (2004).

This left 11 groups, to which we have added a further four groups with data in the *Chandra* archive that conform to the same criteria. The resulting sample includes two Hickson compact groups (HCG 42 and 62) and a fossil group (NGC 741) according to the definition of Jones et al. (2003), and spans a temperature range $kT = 0.3$–2.1 keV, with a median temperature of $T = 1.06$ keV and median redshift of $z = 0.014$. It is worth emphasizing that the selected groups are all reasonably X-ray bright and that the sample is by no means statistically representative. In fact, the invoked net counts criterion alone eliminated 13 of the 25 GEMS systems from which our sample was largely drawn, resulting in a sample lower limit of $L_{\rm X} \approx 5 \times 10^{41}$ erg s^{-1}. Three of our 15 groups are also included in the *XMM* sample of Finoguenov et al. (2006), with a further 6 included in the *XMM* sample of Finoguenov et al. (2007), enabling cross-comparison of the results obtained from the two instruments.

For all our data sets, calibrated event lists were regenerated using CIAO v3.3. For Very Faint mode observations, the standard additional background screening was carried out. Bad pixels were screened out using the bad pixel map provided by the pipeline, and remaining events were grade filtered, excluding *ASCA* grades 1, 5, and 7. Periods of high background were filtered using 3–σ clipping of full–chip lightcurves, binned in time bins of length 259.8-s and extracted in off-source regions in the 2.5–7 keV band for back-illuminated chips and 0.3–12 keV for front-illuminated chips. Blank-sky background data from the calibration database were screened and filtered as for source data, and reprojected to match the aspect solution of the latter.

Point source searches were carried out with the CIAO task 'WAVDETECT' using a range of scales and detection thresholds, and results were combined. Source extents were quantified using the 4σ detection ellipses from 'WAVDETECT', and these regions were masked out in all subsequent analysis. Diffuse emission from individual group galaxies other than the central early-type present in all groups was also masked out.

To provide a rough idea about the spatial distribution of X-ray emission in each system, images of all groups are presented in Fig. 1, showing the adaptively smoothed, background-subtracted and exposure-corrected 0.7–2.5 keV emission on the relevant central CCD (the ACIS-I array for NGC 6338 and NGC 7619, ACIS-S2 for NGC 2300, and S3 for all others). These images were generated following the procedure outlined in Rasmussen, Ponman & Mulchaey (2006). Although small-scale substructure is visible in some of the systems, with the second brightest group galaxy also seen in X-rays in a few cases, most of the groups are evidently reasonably dynamically relaxed, supporting the use of one-dimensional radial profiles to describe the spatial variation in hot gas properties of the systems.

2.2 Spectral fitting procedure

All regions used for spectral extraction were centred on the peak of the diffuse X-ray emission, which in most cases coincided to within 1–2 arcsec (and always within 5 arcsec) with the optical position of the brightest group galaxy as listed in the Hyperleda database. For each CCD in each data set, the appropriate blank-sky data were scaled to match off-source count rates in the 10–12 keV band and then used to generate background spectra. All spectra were fitted in XSPEC v11.3 in the 0.7–5 keV band, with the low-energy cut-off chosen such as to reduce contamination from residual Galactic soft X-ray emission not accounted for by our blank-sky background subtraction (see Section 4 for details). Indeed, no systematic soft residuals between source and background spectra were seen within this energy band for any of the groups.

To put all groups on an equal footing, all radii were normalized to r_{500}, using

$$r_{500}(T) = 0.45 T^{1/2}\ h_{70}^{-1}\ \mathrm{Mpc}, \qquad (1)$$

which is an empirical relation based on data outside the cluster core for a sample of 39 groups and clusters, including eight systems with $T < 1.5$ keV (Finoguenov, Reiprich & Böhringer 2001b). In order to obtain a representative mean temperature $\langle T \rangle$ for use with equation (1), as well as a corresponding mean abundance $\langle Z \rangle$, and to create spectral weights for subsequent fits in individual annuli, a source spectrum was first extracted within the radial range 0.1–0.3 r_{500}. This range was chosen because it extends to the maximum radius covered by ACIS for the more nearby systems, while in all cases being well outside the optical extent of the central galaxy. The latter was quantified as D_{25}, the ellipse outlining a B-band isophotal level of 25 mag arcsec^{-2}. The associated fit results should therefore remain largely uncontaminated by X-ray emission from the interstellar medium and any unresolved point sources in the central galaxy. As we will see, this choice of radial range also excludes any cool core, in accord with our usage of equation (1). The fits to these spectra all adopted an absorbed thermal APEC model in XSPEC, assuming the abundance table from Grevesse & Sauval (1998). Using the derived value of $\langle T \rangle$ with equation (1), r_{500} was then re-evaluated iteratively, until the resulting values of $\langle T \rangle$ varied by less than 1 per cent. Throughout, we will refer to the values of $\langle T \rangle$ and $\langle Z \rangle$ obtained in this way as the mean temperature and abundance of each group.

Spectra were then extracted in concentric annuli containing at least 2000 net counts in the 0.7–1.5 keV band, and accumulated in bins of at least 25 net counts. Spectral response products were weighted by a model of the 'mean' spectrum extracted above. Again, an absorbed APEC model was first fitted to the data, yielding a mean temperature and abundance for the relevant annulus. A second fit was then performed using an absorbed VAPEC model, with all element abundances tied together except for Fe and Si. For spectra extracted inside the region covered by the central early-type galaxy, a power-law of fixed index $\Gamma = 1.72$ was added to the spectral model, to account for any unresolved contribution from low-mass X-ray binaries.

To investigate the presence of multiple thermal components and address the importance of systematic errors associated with the Fe bias (Buote 2000a), we also fitted a 2-T plasma model to all bins inside the optical extent of the central galaxy, with both the Fe and Si abundance tied for the two thermal components. Where either the resulting Fe or Si abundance was significantly different from the 1-T result (at 90 per cent confidence), we adopted the best-fitting 2-T values for both metals, confirming that a 2-T model provided a better fit in all cases. As discussed in more detail in Section 4, this was relevant for only five groups. We note that the adoption of the 2-T results for the abundance in these five cases does not affect $\langle Z \rangle$ significantly, as this quantity has been derived within 0.1–0.3 r_{500}, which is generally well outside the region for which 2-T models provide superior fits in the relevant groups.

Owing to the layout of the ACIS chips, we do not have full azimuthal coverage of the groups at large angular distances from the group centres. Our results at large radii could therefore be sensitive to azimuthal variations in fitted parameters. In an attempt to accommodate the systematic uncertainties associated with this, we used azimuthal variations at smaller radii to gauge the variations further out. For each group, a number of spectra were extracted from an annulus outside D_{25} extending to the maximum radius of full coverage. To mimic the situation at large radii, only data within a narrow strip across this annulus were used, masking out the remaining regions to achieve, if possible, 2000 net counts within the strip, as for the full-coverage annuli. This was repeated a number of times with varying strip position angles. The resulting spectra were then each fitted with a VAPEC model as described above, and the resulting standard variations on relevant parameters (T, $Z_{\rm Fe}$, $Z_{\rm Si}$) adopted as the systematic uncertainties at large radii. The mean uncertainties resulting from this approach were 8, 34, and 58 per cent

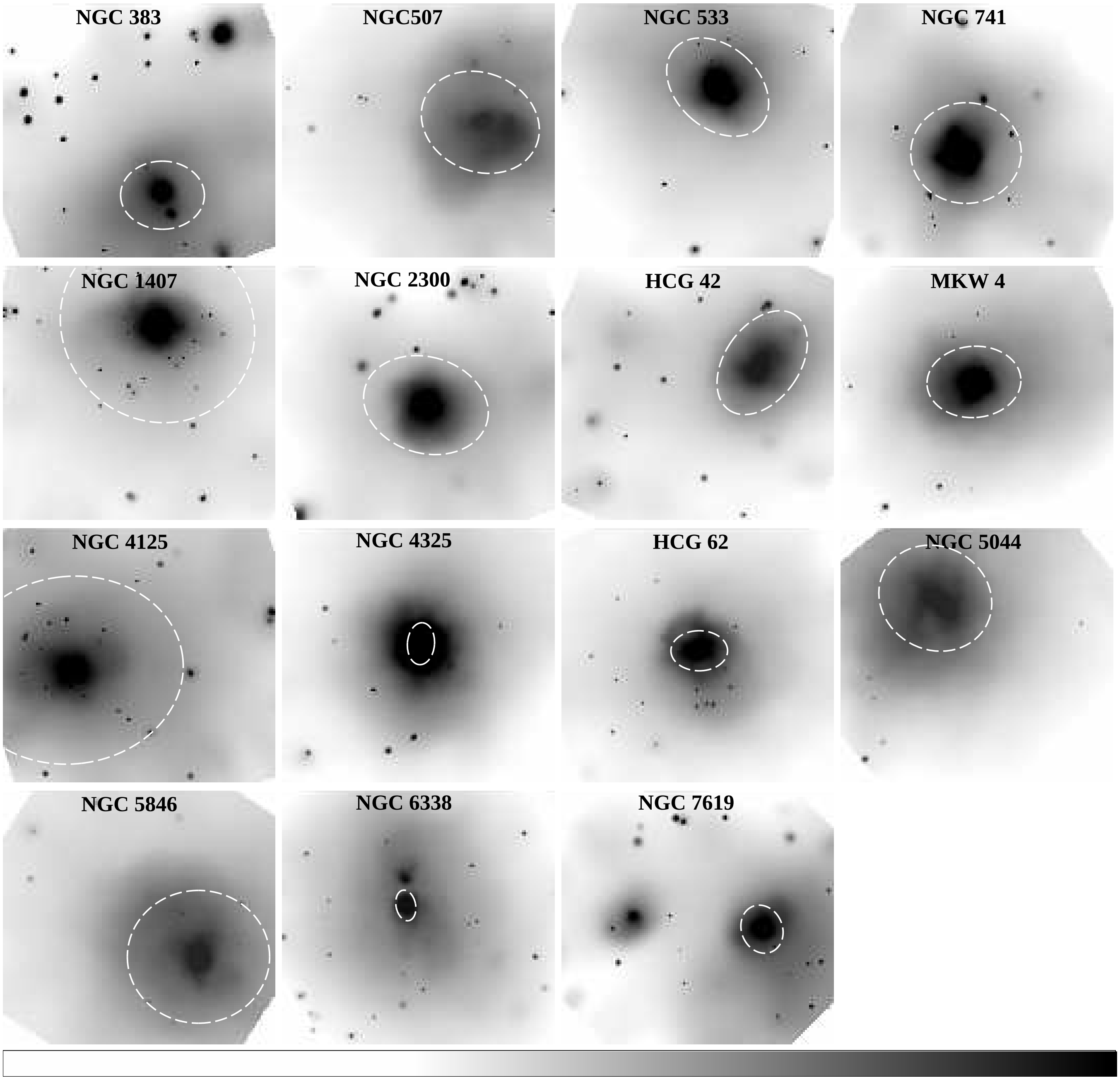

Figure 1. Adaptively smoothed 0.7–2.5 keV images of the central region of all groups. Images of NGC 6338 and NGC 7619 are 14.4 arcmin across, all others 7.2 arcmin. Dashed ellipses outline the D_{25} ellipse of the brightest group galaxy.

on T, $Z_{\rm Fe}$, and $Z_{\rm Si}$, respectively. These errors have been added in quadrature to the statistical errors obtained for all annuli with less than 75 per cent azimuthal coverage (for most groups just one or two radial bins).

Table 1 records the position of the X-ray peak of each group, group distance D corrected for Virgocentric infall, the useful ACIS exposure time $t_{\rm exp}$, $\langle T \rangle$ and $\langle Z \rangle$ from the 'mean' spectrum, r_{500} from equation (1), and the Galactic value of the absorbing column density $N_{\rm H}$ from Dickey & Lockman (1990) as adopted in the fits. Note that the statistical uncertainty on r_{500} based on that of $\langle T \rangle$ alone is typically on the order of just a few per cent. The actual uncertainties on r_{500} are therefore likely to be dominated by systematics associated with the use of equation (1), but a quantification of this is beyond the scope of this paper.

3 RESULTS

In this section we present the results for the projected radial profiles of temperature, Fe and Si abundance, and the ratio $Z_{\rm Si}/Z_{\rm Fe}$. As one of our aims is a statistical investigation of radial trends across the sample, the profiles have not been deprojected, since this would remove the statistical independence of the individual radial bins. However, we discuss the impact of deprojecting the data in Sec-

Table 1. Properties of the group sample.

Group	RA (J2000)	Dec (J2000)	D (Mpc)	$t_{\rm exp}$ (ks)	$\langle T \rangle$ (keV)	$\langle Z \rangle$ ($Z_\odot$)	r_{500} (kpc)	$N_{\rm H}$ (10^{20} cm^{-2})
NGC 383	01 07 24.9	$+32$ 24 45.8	73	42.5	$1.65^{+0.04}_{-0.06}$	$0.39^{+0.07}_{-0.07}$	578	5.41
NGC 507	01 23 39.2	$+33$ 15 19.6	69	14.3	$1.30^{+0.03}_{-0.03}$	$0.40^{+0.07}_{-0.06}$	513	5.23
NGC 533	01 25 31.4	$+01$ 45 33.7	76	33.6	$1.22^{+0.05}_{-0.05}$	$0.28^{+0.07}_{-0.06}$	497	3.07
NGC 741	01 56 21.0	$+05$ 37 42.6	79	28.4	$1.42^{+0.14}_{-0.12}$	$0.16^{+0.08}_{-0.06}$	536	4.44
NGC 1407	03 40 11.8	-18 34 48.9	26	37.7	$1.01^{+0.07}_{-0.09}$	$0.15^{+0.09}_{-0.06}$	452	5.42
NGC 2300	07 32 19.2	$+85$ 42 31.3	30	43.9	$0.78^{+0.04}_{-0.03}$	$0.17^{+0.07}_{-0.05}$	397	5.52
HCG 42	10 00 14.2	-19 38 12.5	64	30.5	$0.80^{+0.05}_{-0.05}$	$0.25^{+0.31}_{-0.10}$	402	4.78
MKW 4	12 04 26.9	$+01$ 53 44.9	96	29.3	$1.78^{+0.07}_{-0.09}$	$0.49^{+0.07}_{-0.07}$	600	1.88
NGC 4125	12 08 05.7	$+65$ 10 27.7	22	60.0	$0.33^{+0.12}_{-0.05}$	$0.19^{+0.17}_{-0.07}$	259	1.82
NGC 4325	12 23 06.7	$+10$ 37 16.0	117	27.9	$0.99^{+0.02}_{-0.02}$	$0.39^{+0.08}_{-0.06}$	448	2.14
HCG 62	12 53 05.8	-09 12 16.0	74	47.1	$1.00^{+0.03}_{-0.03}$	$0.12^{+0.02}_{-0.03}$	450	3.06
NGC 5044	13 15 24.0	-16 23 06.4	33	18.0	$1.12^{+0.03}_{-0.03}$	$0.25^{+0.04}_{-0.03}$	476	4.94
NGC 5846	15 06 29.4	$+01$ 36 23.3	30	22.8	$0.66^{+0.04}_{-0.03}$	$0.16^{+0.06}_{-0.05}$	366	4.24
NGC 6338	17 15 22.9	$+57$ 24 40.5	127	33.5	$2.13^{+0.19}_{-0.07}$	$0.25^{+0.08}_{-0.05}$	657	2.60
NGC 7619	23 20 14.5	$+08$ 12 24.9	52	25.6	$1.06^{+0.07}_{-0.03}$	$0.23^{+0.05}_{-0.05}$	463	5.04

tion 4, showing that this would not compromise our general conclusions.

In order to compare observed abundances and their ratios to those expected from SN Ia and SN II enrichment, we adopted SN model yields taken from the literature. For SN Ia, the currently favoured delayed-detonation WDD2 scenario is assumed (Iwamoto et al. 1999), while for core-collapse supernovae (including types Ib and Ic), we have used the recent yields of Nomoto et al. (2006). The latter were mass-averaged using a Salpeter initial mass function (IMF) for the progenitors over the range 10–50 $M_\odot$ (see Finoguenov, Burkert & Böhringer 2003 and de Plaa et al. 2007 for a justification of this choice of IMF), so that

$$M_i = \frac{\int_{10{\rm M}_\odot}^{50{\rm M}_\odot} M_i(m) m^{-(1+x)}\,{\rm d}m}{\int_{10{\rm M}_\odot}^{50{\rm M}_\odot} m^{-(1+x)}\,{\rm d}m} \qquad (2)$$

is the mass of the i-th element produced in a star of mass m, with $x = 1.35$. We have assumed a fractional metal mass of the SN II progenitors of $Z = 0.004$ (i.e. $Z \approx 0.2$ $Z_\odot$), but the exact choice has no strong bearing on the resulting Fe and Si yields (see, e.g., de Plaa et al. 2007). The resulting average stellar yields are $M_{\rm Fe} \approx 0.79$ $M_\odot$ and $M_{\rm Si} \approx 0.21$ $M_\odot$ for Fe and Si from SN Ia, and $M_{\rm Fe} \approx 0.08$ $M_\odot$ and $M_{\rm Si} \approx 0.12$ $M_\odot$ for core-collapse supernovae including SN II. We note that the yield uncertainties for SN II are substantial, a factor ~ 2 for Fe and ~ 30 per cent for Si; the yields adopted here are bracketed by the results of the different models considered by, for example, Gibson, Loewenstein & Mushotzky (1997), and so can be viewed as representative of typical values in the literature. With the adopted abundance table, the nominal abundance ratios expected for pure SN Ia and SN II enrichment are $Z_{\rm Si}/Z_{\rm Fe} \approx 0.46$ $Z_{\rm Si,\odot}/Z_{\rm Fe,\odot}$ (SN Ia) and 2.62 $Z_{\rm Si,\odot}/Z_{\rm Fe,\odot}$ (SN II). Note that this implies SN II dominance (in absolute numbers) for $Z_{\rm Si}/Z_{\rm Fe} \gtrsim 0.65$, and that a solar abundance ratio requires 3.4 SN II per SN Ia.

By adopting the SN Ia yields of Iwamoto et al. (1999), we restrict ourselves to the 'standard' picture of a reasonably homogeneous population of SN Ia for simplicity. We note, however, that recent developments indicate that the situation could be more complex, with evidence for a diversity in SN Ia yields in cluster cores (Finoguenov et al. 2002) and for two distinct populations of SN Ia (Mannucci, Della Valle & Panagia 2006).

3.1 Temperature profiles

Radial temperature profiles for all groups derived from single-temperature models are presented in Fig. 2, with the radii of all annuli normalized to r_{500}. It is worth noting that emission is detected to fairly large radii in most of the groups, with the midpoint of our outermost radial bin corresponding to roughly 75 per cent of r_{500}. This can be ascribed to the relatively low and stable *Chandra* background.

In general, the temperature profiles appear remarkably similar, with all but one system (NGC 4125) showing evidence for cooler gas in the central regions. The temperature profiles typically peak around $r \sim 0.1 r_{500}$ and decline at large radii. There is also an indication that the profiles flatten in the central regions, in general agremeent with the group results of Finoguenov et al. (2007). Compared to analogous profiles for relaxed clusters, this contrasts with the projected *Chandra* temperature profiles of Vikhlinin et al. (2005), the deprojected ones of Sanderson et al. (2006), and the deprojected *XMM* profiles of Piffaretti et al. (2005), for which there is no clear evidence for a flattening at small radii. Defining the gas entropy as $S = T n_e^{-2/3}$, the deprojected cluster entropy profiles of Donahue et al. (2006) *do* show a central flattening, but this was attributed to a central core in the density distribution rather than a flattening of the temperature profile.

The typical location of the temperature peaks in our sample is in excellent agreement with the *XMM* results of Gastaldello et al. (2005), who also found temperature peaks at $r \sim 0.1 r_{500}$ for their cool-core groups and poor clusters. Their sample has four groups in common with ours (NGC 533, MKW 4, NGC 4325, and NGC 5044), and has r_{500} evaluated directly from the mass profiles derived for each group. The good agreement with our results therefore also suggests that our estimates of r_{500} are generally not seriously biased. As also noted by Gastaldello et al. (2005) for their sample, the temperatures peak at larger overdensity than in clusters, where the profiles turn over at $r \approx 0.15 r_{500} \approx 0.1 r_{200}$ (Piffaretti et al. 2005; Vikhlinin et al. 2005; Zhang et al. 2006; Sanderson et al. 2006). It is clear, however, even when nor-

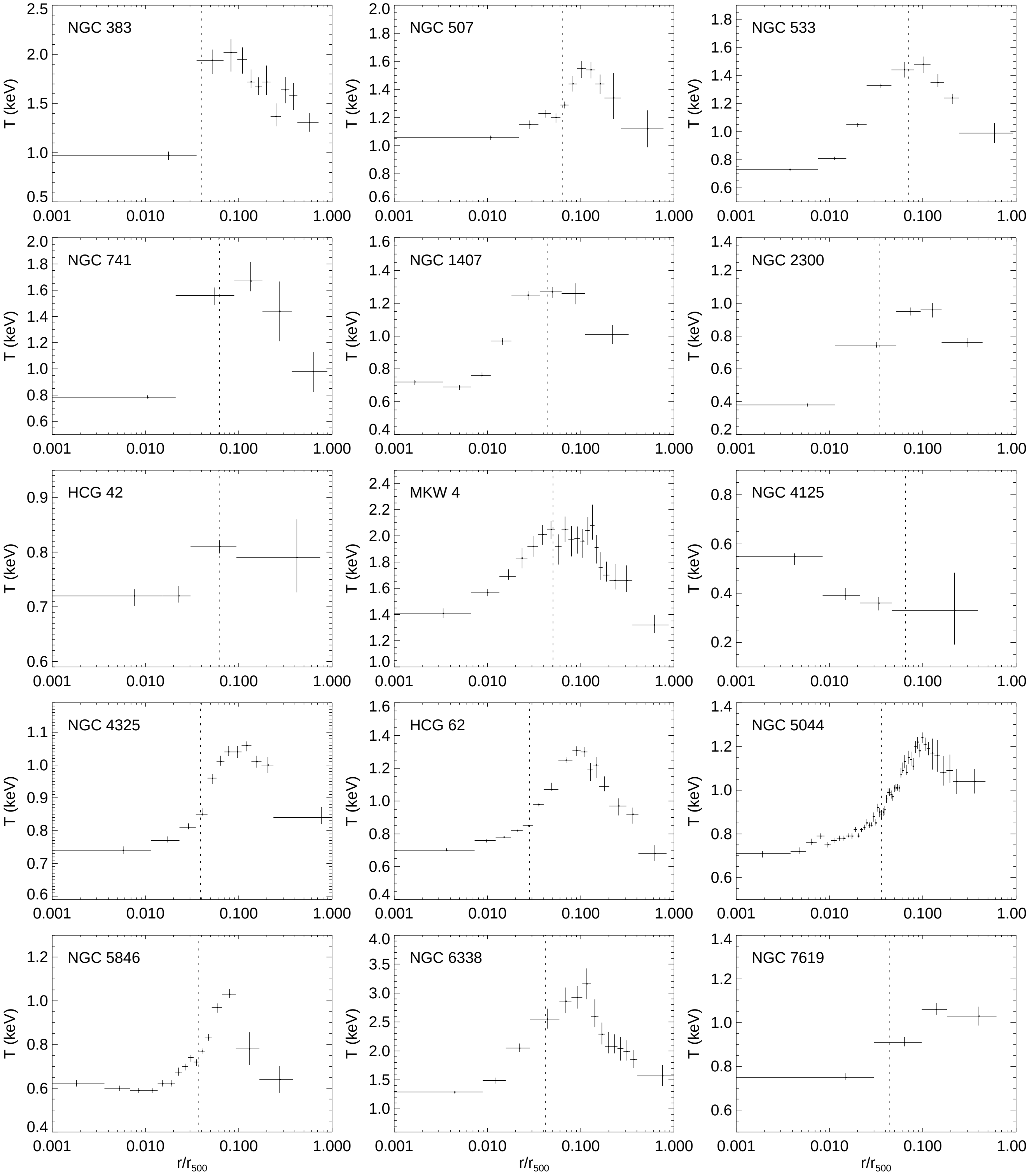

Figure 2. Projected radial temperature profiles of all groups. Vertical dotted lines mark the semi-major axis of the D_{25} ellipse of the central group galaxy.

malized to r_{500}, that the exact radius $r(T_{\rm max})$ at which the peak occurs (in other words, the radial extent of the cool core) varies slightly from group to group. Naturally, this result will to some extent depend on the spatial resolution resulting from our binning criterion and thus the surface brightness of the group emission, but we note that the adopted spatial resolution does not depend systematically on, for example, group temperature. We discuss the location of the temperature peak in more detail in Section 5.1.

3.2 Abundance profiles

The abundance profiles of Fe and Si are plotted in Fig. 3. In all systems except NGC 2300, and possibly the non–cool core group NGC 4125, there is clear evidence for a central excess of iron, as also seen for cool-core clusters. This central excess often extends well beyond the optical extent of the central galaxy, and in some cases shows an off-centre peak inside D_{25}, with a decline in abundance in the very centre. NGC 533 is perhaps the clearest example of this, but the majority of groups with a well-resolved core (roughly 8/11) shows some evidence of this feature. This Fe peak is typically accompanied by a similar feature in the Si distribution, most clearly in HCG 42, MKW 4, and HCG 62, with a hint of similar behaviour in a few more groups. Potentially, the peak could be ascribed to Fe/Si bias inside the central galaxy, lowering the derived abundance in the very core, but as discussed below, we find little evidence that this effect is important for our analysis in general. In addition, such a peak is commonly seen also in well-resolved cluster cores where the Fe bias is generally expected to be less important, e.g., Centaurus (Sanders & Fabian 2002), Perseus (Sanders, Fabian & Dunn 2005), A1795 (Ettori et al. 2002), and A2199 (Johnstone et al. 2002). Alternative explanations for the peak include AGN redistribution of enriched gas (e.g., Mathews et al. 2003; Rebusco et al. 2006), resonant scattering of emission line photons in group cores (Gilfanov, Sunyaev & Churazov 1987), or gravitational sedimentation of helium nuclei in the core (Ettori & Fabian 2006). We will discuss these possibilities in detail in Paper II.

At large radii, a common feature of the Fe distributions is a drop in $Z_{\rm Fe}$ to a value of ≈ 0.1 Z$_\odot$. In some groups, a rise in $Z_{\rm Si}$ is also seen, largely independent of the behaviour of the Fe profile. We note that there is no indication that derived profiles for the two Hickson groups or the fossil group NGC 741 differ significantly from those of the rest of the sample in this context.

The silicon-to-iron ratio $Z_{\rm Si}/Z_{\rm Fe}$ is plotted for all groups in Fig. 4. In many cases the ratio in the central bin is seen to be consistent with the Solar ratio, with a contribution from SN II formally required for about half the groups. For the other half, there is clear evidence for subsolar abundance ratios, consistent with enrichment by SN Ia alone. We do not believe there is any fundamental difference between the two subsamples if split according to this, as $Z_{\rm Si}/Z_{\rm Fe}$ in the central bin clearly spans a continuous range of values rather than showing a bimodal distribution. Given the variation in spatial resolution among the groups and the uncertainties on $Z_{\rm Si}/Z_{\rm Fe}$, we caution further against such an interpretation at this stage. For example, we find no evidence that the two subsamples cluster differently in the parameter space spanned by $\langle T\rangle$, $\langle Z\rangle$, and K-band luminosity of the central galaxy. Nevertheless, we will revisit this issue in Paper II on the basis of integrated Fe and Si masses inside D_{25}.

As discussed by Finoguenov et al. (2002), there is observational evidence for diversity in SN Ia yields in the cool cores of more massive clusters, with solar Si/Fe ratios arising entirely from SN Ia. While our results allow for this possibility, we cannot easily confirm that this result extends down into the group regime, as it is based on the abundances of additional elements such as S, Ca, and Ar. At the lower temperatures prevalent in groups, the abundances of these elements, with prominent emission lines in the range $E \approx 2.5-5$ keV, are not in general robustly constrained. In the outer regions, the interpretation of our data remains unaffected by this; here a contribution from SN II is universally required within our sample, and the abundance ratios, given the typical uncertainties in SN II yields of a factor ~ 2 (e.g. Gibson et al. 1997), are consistent with pure SN II enrichment in all cases.

3.3 Notes on individual systems

Many of the groups exhibit properties which warrant some additional comments. Below, we briefly discuss each group in the sample in turn, with emphasis on the derived abundances. Where relevant, we have also attempted a comparison of the derived Fe profile to existing measurements, in particular the 2-D *XMM* results of Finoguenov et al. (2006, 2007) (F06 and F07 in the following), while correcting for differences in adopted abundance tables. It should be noted, however, that due to our incomplete azimuthal coverage at large radii, direct comparison is not always straightforward for sources with some degree of asymmetry in the Fe distribution.

NGC 383: The central galaxy hosts the bright radio source 3C 31, representing one of the few examples of a central group galaxy showing a clearly identified large-scale radio jet with a well-constrained jet power (Laing & Bridle 2002). Despite this, the T– and Z-profiles of this group do not exhibit any clear distinguishing features compared to the rest of our sample. For the temperature profile, this result is in accord with the group results of Jetha et al. (2007), which show that the slope of $T(r)$ inside the cool core does not show any strong dependence on the radio power of the central radio source.

NGC 507: An example of a group in which radio lobes are present around the central galaxy (Kraft et al. 2004) and in which the highest-metallicity gas is displaced from the group core, perhaps as a consequence of radio outbursts lifting enriched gas out of the core. If so, one might expect to see some degree of asymmetry in the Fe distribution in the core. The 2-D Fe map of F07 does reveal some asymmetry inside $0.05r_{500}$, showing a high-metallicity blob south-west of the group core, but it is not immediately obvious that this is necessarily associated with an AGN outflow. To achieve a satisfactory fit in the outermost radial bin in our data, it was necessary to exclude the second brightest group galaxy, NGC 499, out to 6 arcmin ($\sim$ 120 kpc). Comparison to the single-T Fe profile of F07 shows good overall agreement, including the off-centre Fe peak at $\sim 0.03r_{500}$ and the decline to ~ 0.3 Z$_\odot$ at $0.5r_{500}$.

NGC 533: This group presents one of the clearest examples of an off-centre peak in the Fe distribution within our sample. As for NGC 507, which also hosts such an Fe peak, 1.4-GHz NVSS data (Condon et al. 1998) reveal a central radio source. Inside $0.02r_{500}$ our Fe results are consistent with the F07 value of ~ 0.7 Z$_\odot$, as is our detection of the supersolar Fe peak at $0.04r_{500}$. The clear decline to 0.1 Z$_\odot$ at large r is not obvious from the F07 results, however, which show considerable scatter outside $0.1r_{500}$. We speculate that this relates to our assumption of circular symmetry and our incomplete azimuthal coverage at large radii. The 2-D Fe map of F07 suggests an elongated abundance structure on large scales, with the ACIS-S array in our *Chandra* data running very nearly perpendicular to the major axis of this structure. This implies that our result includes low-metallicity gas at the largest radii, beyond those included in the F07 analysis, and that we are inevitably missing some of the higher-metallicity gas seen by F07.

NGC 741: With a group X-ray luminosity of 3×10^{42} erg s^{-1} (Osmond & Ponman 2004), and a B-band magnitude differ-

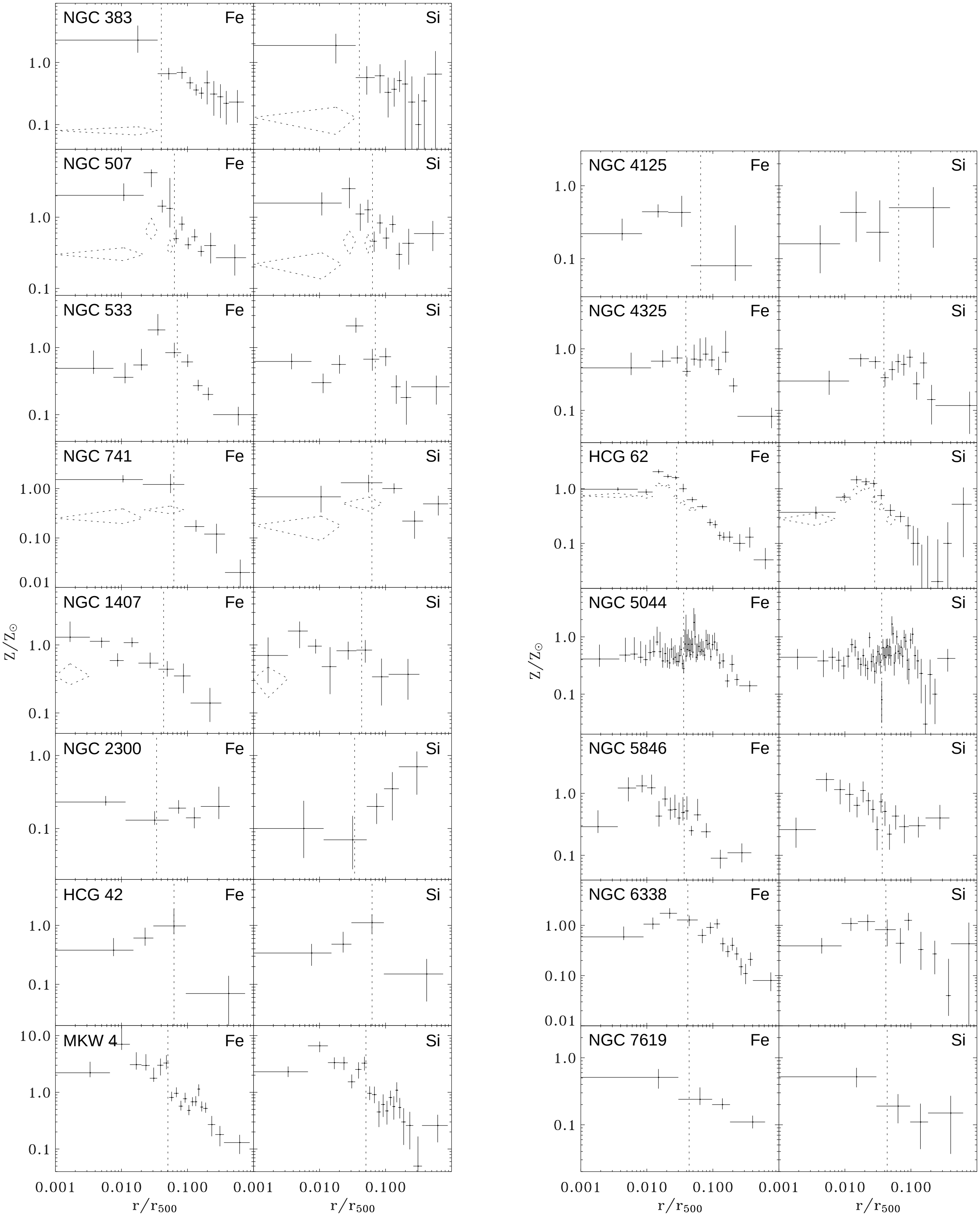

Figure 3. As Fig. 2, but for the Fe and Si profiles. Where relevant (see Section 2.2), the result of fitting two-temperature models have been plotted, with the corresponding 1-T results shown as dotted diamonds.

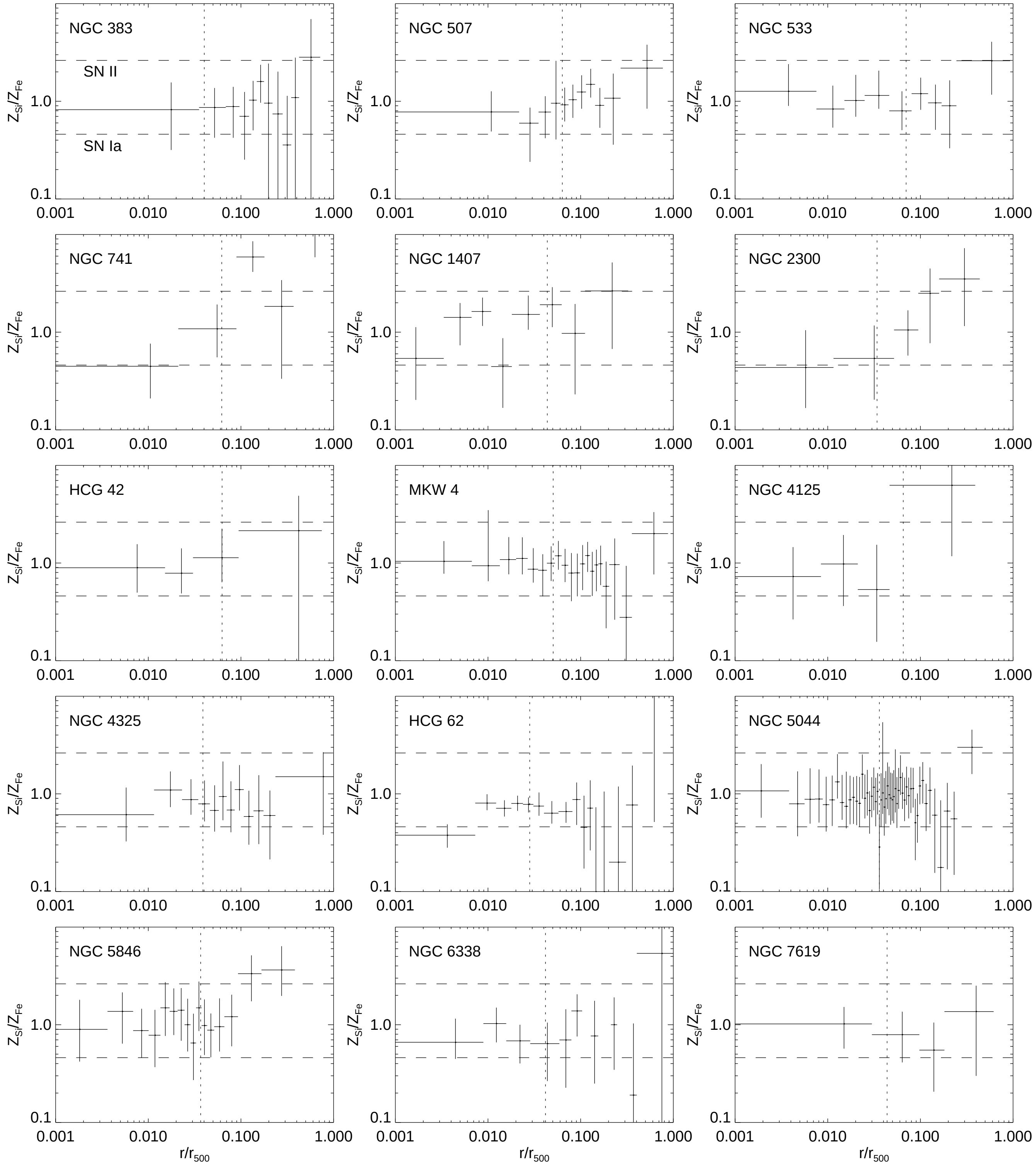

Figure 4. As Fig. 2, but for the ratio of $Z_{\rm Si}/Z_{\rm Fe}$ (in units of $Z_{\rm Si,\odot}/Z_{\rm Fe,\odot}$). The lower and upper dashed lines mark the ratios expected from pure SN Ia and SN II enrichment, respectively.

ence between the first and second brightest galaxy (the spiral UGC 1435) within r_{500} of $\Delta m_{12} = 2.6$, this system meets the criteria for fossil groups introduced by Jones et al. (2003). Its temperature and metallicity profiles appear similar to those of most other systems studied here, though the Fe abundance at large radii is clearly lower than average. It is also a group with a powerful central radio source and large-scale radio emission (e.g., Jetha et al. 2007), although the latter is probably a tailed radio source associated with the nearby group member NGC 742 rather than with the central elliptical itself (Jetha et al., in prep.).

NGC 1407: This is probably a dynamically evolved group, with overall optical properties not too dissimilar to those of the fossil system NGC 741 (Trentham, Tully & Mahdavi 2006). Its Fe and Si profiles appear fairly typical for the sample.

NGC 2300: This is the only group within our sample with a spatially resolved Fe profile outside D_{25} that does not show clear evidence for a radial decline. The Si profile is also somewhat atypical of the sample, showing a clear rise with radius outside the core. The relatively low and near–constant Fe abundance, as well as the radial rise in Si, is in very good agreement with earlier *ROSAT* and *ASCA* results (Davis et al. 1996; Finoguenov et al. 2002), although the *XMM* study of F06 seems to find slightly higher Fe abundances inside $0.3r_{500}$ than those seen here. With the central early-type galaxy (NGC 2300 itself) having a stellar mass $\sim$ 10 times that of the second largest galaxy, NGC 2276 (Rasmussen et al. 2006), the central galaxy could potentially have been almost solely responsible for the chemical enrichment of the hot gas in this system. This is also an example of a group in which ram-pressure stripping of (presumably enriched) galactic gas is taking place (Rasmussen et al. 2006), illustrating that an SN–driven outflow is not the only mechanism for enriching the hot gas in the group. We note that there is also evidence of a recent merger in the central early-type (Forbes & Thomson 1992), with further evidence for this seen in the ICM pressure map of Finoguenov et al. (2006).

Given that other features of this group seem typical of our sample, such as the presence of a cool core and a fairly undisturbed X-ray morphology, the question remains how to interpret the uniformly low Fe abundance and the rise in $Z_{\rm Si}$ with radius. We note that $Z_{\rm Fe}$ at large radii is not atypical of the sample, nor is the radial profile of Si/Fe. This suggests a suppression of both Fe and Si enrichment in the group core. In light of the evidence of a recent merger in the central early-type, one possible explanation is that a cool, low-Z system has dropped into the group core, thus diluting any Fe excess but preserving the cool core.

Another possibility, potentially induced by the very low central temperature, is that high-Z gas has cooled out in the group core. Based on the measured X-ray flux, the fitted spectral parameters, and the gas density profile of Davis et al. (1996), we estimate a central cooling time of only $\sim 1 \times 10^8$ yr. This would render such cool-out a viable scenario, in particular in light of the absence of any strong radio source in the central early-type (1.4 GHz radio power $P \approx 5 \times 10^{20}$ W Hz^{-1} based on the NVSS flux) which could indicate ongoing AGN heating activity. In order to remove any Fe excess and explain the 'suppressed' Fe level in the core, a total Fe mass of 2.5×10^5 M$_\odot$ must have cooled out inside the typical radial extent of the Fe excess of $r \approx 0.05r_{500}$, assuming an initial Fe abundance of $\sim$ 0.7 Z$_\odot$ (see Section 5 for this choice of parameters). This is equivalent to a total gas mass of 2.0×10^8 M$_\odot$, which does not seem an unreasonably large amount. In addition, cooling would also have raised the central entropy through the removal of low-entropy gas from the X-ray phase. Among the nine of our groups also included in the F06 and F07 samples, NGC 2300 does show the highest central entropy, lying 1.6σ above the sample mean derived inside $0.1r_{500}$ (F06). One concern for the cooling scenario, however, is that the cooled gas is likely to participate in star formation (Edwards et al. 2007), but there is no indication that the central early-type is unusually blue, displaying a B–K colour of 4.2. Based on the X-ray data alone, we conclude that the cooling scenario provides a possible explanation for the lack of an Fe excess in this group, but further tests of this would require constraints on the amount of cold gas and young stars in the central early-type galaxy.

HCG 42: The observed range of $Z_{\rm Fe} = 0.5 - 1.0$ Z$_\odot$ inside $0.1r_{500}$ is consistent with the F07 results, as is the decline at large radii. However, finding a low value of ~ 0.1 Z$_\odot$ outside the cool core, we do not confirm the value of 0.2 Z$_\odot$ seen in the outermost bin of F07, certainly in part because we do not have the statistics required to resolve this narrow region around $0.5r_{500}$.

MKW 4: The presence of an off-centre Fe peak in this group was already claimed by Fukazawa, Kawano & Kawashima (2004), who furthermore noted that no radio activity or merger evidence has been reported for the system. Indeed, NVSS data show no evidence of a central radio source, nor of any larger-scale radio emission surrounding the central galaxy, NGC 4073 (Jetha et al. 2007). This is in clear contrast to NGC 507 and NGC 533, where this Fe peak is accompanied by the presence of a central radio source. We confirm the high central Fe abundance of ~ 2 Z$_\odot$ seen by F07, along with the sharp decline, starting at $0.05r_{500}$, towards a value of 0.1 Z$_\odot$ at large radii.

NGC 4125: This group is the lowest-temperature system in the sample. It shows no cool core, despite appearing reasonably relaxed in the X-ray (Fig. 1). Subdividing the innermost radial bin and fitting spectra for each sub-bin, each only ≈ 500 pc wide, still does not reveal any temperature drop. As there appears to be a point-like X-ray source at the centre, detected above the local background at $\sim 2\sigma$ significance, one possibility is that the central temperature rise could be due to recent AGN heating. However, although a radio source is present in NVSS data inside D_{25}, this source is displaced from the optical and X-ray centre by 0.8 arcmin (4 kpc). To investigate the nature of the central X-ray source, its spectrum was fitted with a power-law absorbed by the Galactic value of $N_{\rm H}$. This provided an unacceptable fit, even when allowing for intrinsic absorption beyond the Galactic value (red. $\chi^2 > 1.7$ for 9 degrees of freedom). In contrast, an APEC plus power-law model fits well (red. $\chi^2 \approx 0.6$), yielding $T = 0.56 \pm 0.12$ and $Z = 0.39^{+0.34}_{-0.18}$ for the thermal plasma, and $\Gamma \approx 1.7$ for the power-law, with a total, unabsorbed luminosity of 1×10^{39} erg s^{-1}. The plasma parameters are in good agreement with those found on larger scales in the group core, and the power-law with a contribution from low-mass X-ray binaries in the central elliptical. The *Chandra* detection of a central point source might therefore simply be attributed to a strongly peaked surface brightness profile, in line with the *ROSAT* finding of Mulchaey et al. (2003) for this group. We therefore conclude that there is no strong X-ray evidence for ongoing AGN heating having raised the central ICM temperature. Further support for this interpretation is provided by the low X-ray luminosity derived for the very central regions, which is well below typical AGN luminosities.

An alternative explanation for the central temperature rise could be sought in the fact that the central elliptical is 'dynamically young' (Fabbiano & Schweizer 1995), so a merger event within the past few Gyr could have disturbed the central regions and mixed in hotter gas from larger radii. The derived central cooling time is very short, however, $\sim 1 \times 10^8$ yr as for NGC 2300, but increasing to more than 3 Gyr at D_{25} as a consequence of the sharply peaked surface brightness, and hence density, profile (Mulchaey et al. 2003). As this is a factor of three above the sound crossing time within that region, it may suggest that the gas density distribution has largely recovered from such a merger disturbance, but significant central cooling has yet to commence.

Another possibility is that the situation in NGC 4125 is somewhat similar to that seen for the fossil group NGC 6482, one of the coolest known fossils, with a temperature of only ≈ 0.5 keV outside the central 10 kpc (Khosroshahi, Jones & Ponman 2004). Despite looking relaxed in the X-ray and displaying a central cooling time of $\lesssim 10^8$ yr, this system also shows no cool core. A possible explanation is that any gas taking part in a steady-state cooling flow in this group is actually *heated* by gravitational PdV work as it moves inwards, owing to the very cuspy total mass profile of the group. Khosroshahi et al. (2004) find that, in such a scenario, the observed temperature profile can be explained by a cooling-flow mass accretion rate of just 2 $M_\odot$ yr^{-1}. The sharply peaked density profile seen for NGC 4125 is consistent with the idea that a similar mechanism could be at work in this group.

NGC 4325: This is a group in which the extent of the metal excess in the core substantially exceeds the optical extent of the central galaxy. No central radio source is seen in NVSS data (Jetha et al. 2007), but there is evidence of a previous weak AGN outburst, with an indication that another outburst may be about to occur (Russell, Ponman & Sanderson 2007). The observed near-constancy of $Z_{\rm Fe} \approx 0.7 - 0.8$ Z$_\odot$ inside $0.1r_{500}$ agrees well with the F07 results, as does the very steep decline to a value $Z_{\rm Fe} < 0.1$ Z$_\odot$ at $0.8r_{500}$.

HCG 62: This group has been extensively studied with *ROSAT*, *ASCA*, *Chandra*, and *XMM* (Finoguenov & Ponman 1999; Buote 2000b; Morita et al. 2006). It harbours one of the clearest examples of X-ray cavities in groups (Vrtilek et al. 2000; Morita et al. 2006), indicating past radio activity. The older CIAO task 'MKRMF' was used to create spectral responses for this group, due to a lack of relevant calibration data for the newer task 'MKACISRMF' otherwise used in this study. Despite this and the complex X-ray morphology in the core of this system, the combined *Chandra* and *XMM* study of Morita et al. (2006) finds a temperature profile very similar to the one derived here, and the roughly solar Fe and Si abundances seen in the core agrees well with the results of Buote (2000b) and Morita et al. (2006). The sharp decline in the Fe profile, beginning at $\sim 0.03r_{500}$ and reaching a value of ~ 0.05 Z$_\odot$ at $0.6r_{500}$, is also in good agreement with F07.

NGC 5044: This system has been studied extensively with both *XMM* and *Chandra* (Buote et al. 2003a,b; Buote, Brighenti & Mathews 2004). At $r \approx 0.05r_{500}$, our results are consistent with the solar Fe abundance found by F06. In our outermost radial bin, we find $Z_{\rm Fe} = 0.14 \pm 0.04$ Z$_\odot$, confirming the low Fe abundance of 0.1–0.15 Z$_\odot$ derived at large radii by Finoguenov & Ponman (1999) and Buote et al. (2004).

NGC 5846: The Fe map of F06 suggests a highly symmetric abundance structure, and supports our detection of an off-centre Fe peak and a decline to 0.1 Z$_\odot$ at large radii.

NGC 6338: Reaching a peak temperature of $T \approx 3$ keV, this is the hottest system in our sample. In Fig. 1, extended emission is also seen from the second brightest galaxy. This has been masked out to a radius of 1 arcmin in all spectral fits. As for NGC 4325, the central metal excess in this group extends well beyond the central galaxy, but is here also accompanied by a central radio source.

NGC 7619: NGC 7619 itself is one of a central pair of ellipticals of similar optical brightness in the group. Extended X-ray emission is also seen in Fig. 1 around the other pair member, NGC 7626; this was masked out to a radius of 2 arcmin in all spectral fits.

4 SYSTEMATIC ERRORS

Before proceeding to discuss the results in more detail, we address a number of analysis issues which could be affecting our results. These include the presence of Fe and Si biases in the group core, and the reliability of our background estimates. An immediate, although indirect, indication that such issues are not having a major impact on our results, is the fact, discussed below, that we detect the same overall radial trend in T and Z for all systems, despite considerable variations in both source and background flux across the sample. For the temperature profiles, the agreement with the *XMM* result of Gastaldello et al. (2005) for the mean position of the temperature peak is encouraging. Moreover, there is good overall agreement with derived Fe profiles for the six groups overlapping with the *XMM* sample of Finoguenov et al. (2007), even at large radii where systematic uncertainties related to background subtraction could be important.

4.1 Geometric effects

One issue which could call the robustness of our results into question is the fact that our profiles are projected ones, so all bins contain some contribution from emission further out. To test the importance of this effect, we deprojected the profiles for a few groups using the PROJCT model in XSPEC. For simplicity, a 1-T APEC model was fitted to the data. The result for NGC 4325 is shown in Fig. 5. This group is typical of our sample in terms of the number of radial bins and the value of $\langle T \rangle$; it also shows a near-solar Si/Fe ratio throughout, so the measurements should not be biased strongly by fixing the relative abundances. The figure demonstrates reasonable overall agreement between projected and deprojected results. As can be seen, projection tends to slightly reduce the temperature gradient in the core, as would be expected. While the deprojected abundance profile recovers the increased Fe level in the region inside $\sim 0.1r_{500}$, significant fluctuations between adjacent bins are evident in this region in disagreement with the projected profile. These are most likely artefacts related to issues of fit stability, a problem commonly arising for spectral deprojections involving a large number of bins (e.g., Sanderson et al. 2006). Results for less well-resolved systems support this suspicion and confirm the lack of systematic variations between projected and deprojected results. We therefore conclude that our results are reasonably reliable representations of the three-dimensional profiles.

Another issue is the fact that we have incomplete azimuthal coverage at large radii. This could potentially play a role for individual groups in which a simple radial description of the abundance profile breaks down in the outskirts. As mentioned, however, we have attempted to select systems with a reasonably regular X-ray morphology, and we have also tried to accommodate any remaining uncertainties related to this in our error analysis. The good overall agreement with *XMM* results at large radii indicates that this effect is not important, at least for the groups where a comparison is possible. In addition, any bias would be strongly suppressed when averaging the results across the group sample, which is the approach taken in the next Section. We therefore believe our conclusions to be robust against this effect.

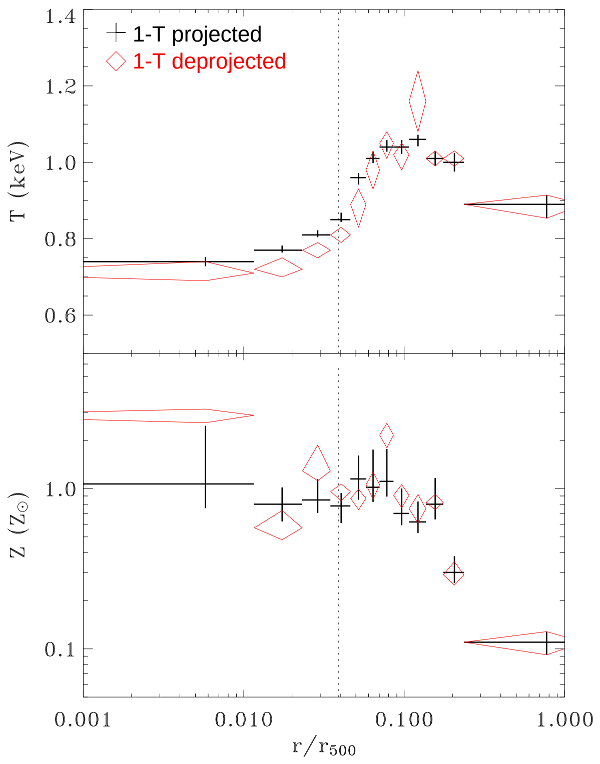

Figure 5. Projected and deprojected temperature and abundance profiles for NGC 4325, resulting from fitting a single-temperature model to all bins.

4.2 Observational bias in group cores

It is well known that high-quality observations of groups in many cases reveal disturbed central structures, showing that group cores can be thermally complex (e.g. Kim & Fabbiano 2004; O'Sullivan et al. 2005) and require multi-component thermal models to properly fit their spectra. To investigate this, we plotted the distribution of reduced χ^2 values for all our fits, but found no clear trend with radius and no indication that multi-temperature models are generally *required* to describe the central regions.

Nevertheless, particularly for systems such as NGC 383, where the central cool regions are not well resolved because of our binning criterion, the presence of multi-phase gas could lead to artificially low abundance estimates in the innermost bin (Buote 2000a), and metallicities derived from 1-T fits should here be regarded with some caution. We tested for this effect by first radially subdividing the central radial bin and fitting spectra extracted within each of these two sub-bins. Eight of the 15 groups show evidence for T variations between those two sub-bins. For all systems, the abundance values within the two sub-bins were consistent with the full-bin value, and only one group displays evidence for Z variation between the two sub-bins (NGC 383, with the innermost sub-bin showing a lower value). However, this does not in itself rule out the presence of multi-phase gas within each of these two sub-bins. A further test therefore involved fitting two-temperature models to all bins within D_{25}, as already described in Section 2.2. Only for five groups do we find evidence that 2-T models yield significantly higher abundances *and* provide superior fits, in some of the innermost radial bins (Fig. 3). For these, the 2-T results for the abundances have been adopted, as plotted in Fig. 3. An example is NGC 507, for which only the 2-T fit recovers the high Fe abundance of 2–3 Z$_\odot$ reported inside D_{25} by Kim & Fabbiano (2004) on the basis of *XMM* data.

While 2-T models certainly provide better fits in some cases, it is perhaps slightly surprising that they only yield significantly different abundances in a few of these, given the presence of central temperature variations in most of our groups. A possible explanation is that we are typically sampling the core regions with rather finely spaced annuli. The limited radial extent of each annulus may imply that mixing of temperature components may not be important within each bin. For example, for the very core of MKW 4, Fukazawa et al. (2004) also find from the same *Chandra* data that 2–T models do not produce significantly improved fits or higher $Z_{\rm Fe}$, in agreement with our results. A different conclusion was reached by O'Sullivan et al. (2003) based on *XMM* data, which Fukazawa et al. (2004) attribute to the much larger spectral extraction region used by the latter authors. Support for this interpretation is provided by the work of Humphrey & Buote (2006), which shows that *Chandra* spectra of elliptical galaxies can generally be described by 1-T models, and that the multi-T fits required to describe earlier *ASCA* spectra of the same objects were an artefact of sampling strong temperature gradients with poorer spatial resolution. The fact that we generally find 2–T models to yield better fits and higher abundances only for groups where our innermost bin covers a large fraction of D_{25}, would seem to add support for this interpretation. Indeed, as discussed in Paper II, for spectra covering the full region inside $0.1r_{500}$ (a region much larger than that covered by the central bin in all groups), we find that two-phase models are in most cases statistically required. In addition, we note that the introduction of a $\Gamma \approx 1.7$ power-law to account for unresolved X-ray binaries in the central early-type also mitigates the need for a 2-T model in some cases.

It is finally worth noting that any remaining Fe bias would only strengthen the result that an Fe excess is present in the cores of most of our groups. Qualitatively, therefore, the only significant feature potentially induced by the Fe bias would be the off-centre Fe peak seen in some systems. However, some of our groups for which 2–T models provide better fits and significantly enhanced abundances in the central regions, such as NGC 507, still show evidence for such Fe and Si peaks, suggesting this feature is reasonably robust to such a bias.

4.3 Background estimation

Another important issue is the accuracy of our background subtraction. This is mainly relevant at large radii, where the emission at all energies is typically dominated by the background. As mentioned, we use blank-sky data to extract background spectra, scaled to match the 10–12 keV count rates of our source data for each CCD. The resulting medium-to-hard background above $E > 4$ keV seems properly accounted for in all cases, as there is no statistically significant residual emission above this energy within the spectral extraction regions employed for *any* data set. Of potentially more concern is the soft X-ray background below $E \approx 1$ keV, whose intensity varies considerably across the sky. For 10 out of our 15 groups, the *ROSAT* All-Sky Survey $R45$ (0.5–0.9 keV) background count rates are within 2σ ($\lesssim 10$ per cent deviation) of the analogous value for the relevant blank-sky background data, lending support to our use of the latter for background estimation. While most of our groups are thus not projected onto regions of significantly enhanced or depleted soft X-ray background, there are a few exceptions which all show enhanced background, most notably

NGC 5044 and NGC 5846 which both lie close to the North Polar Spur.

For most of our systems, intragroup emission covers the field of view (r_{500} is outside the field of view in most cases), so we cannot in general use the outer portions of the observed fields to reliably assess the level of any residual soft background. Instead, two independent tests were performed to assess the impact of varying the assumed background: We either simply rescaled the blank-sky background, or added a separate background model component in the fits to the group emission.

In the first test, we repeated all fits for the three outermost radial bins of each group, with the blank-sky background normalization shifted by ± 10 per cent. The fits were performed in the 0.7–2.0 keV band only, to prevent the obvious mismatch resulting at higher energies from affecting the results. We found that this in general induced negligible changes in the best-fitting temperature, which remained consistent with the value derived for the 'unperturbed' background in all but two cases (when increasing the background for NGC 4125 and NGC 6338), for which the resulting fits were statistically unacceptable anyway. If anything, the best-fitting value of T is slightly lower in all cases, so there is no indication that the temperature decline observed in all groups at large radii can be ascribed to inaccurate background subtraction. We therefore conclude that the large-scale behaviour of the temperature profiles in Fig. 2 is a robust result.

The resulting abundances are more sensitive to variations in the assumed background level. For three of the groups (HCG 42, NGC 1407, and NGC 2300) rescaling the background produced higher abundances in the outermost bin, inconsistent with the result obtained using our standard background level. None of these cases yielded unacceptable fits, so we conclude that significantly higher values of Z in the outermost region probed for these systems are allowed, though not favoured, by the data. However, at least in the case of HCG 42, there is good reason to believe that the existing abundance measurement is fairly reliable, as it compares well to the result derived independently from *XMM* data (Finoguenov et al. 2007). Similar agreement is found for NGC 2300 when compared to earlier *ROSAT* and *ASCA* results (see Rasmussen et al. 2006). As an additional test, we also tried varying the background normalization by ± 20 per cent for all groups. In the four cases where the resulting fits did not become either significantly worse or statistically unacceptable, the derived T and Z were consistent with the results obtained using the unperturbed background.

As a second test, carried out for the five groups with significantly enhanced soft background, we included a spectral model to account for this excess background, and repeated all fits outside the cool core with this model added to that used to describe the group emission. Following Vikhlinin et al. (2005) and O'Sullivan et al. (2007), a fixed $T = 0.18$ keV, $Z = \mathrm{Z}_{\odot}$ MEKAL background model was assumed, with only its normalization allowed to vary. Only for NGC 5846, which – along with NGC 5044 – shows the highest background excess, did we find significant changes in fitted parameters, with this (improved) fit yielding lower Fe and Si abundances, which we have consequently adopted. For NGC 5044, no changes were seen, possibly because of the relatively high signal-to-noise ratio in the outermost bins for this group.

We confirmed that soft background excess is not an issue for the remainder of the sample. For example, for relatively compact low–surface-brightness sources such as HCG 42 and NGC 4125, there is no statistically significant residual emission in the 0.7–2 keV band in a 2 arcmin wide annulus extending to the edge of the field of view. For the adopted soft background model, only 15 per cent of the total 0.5–0.9 keV flux (used to determine the presence of a soft excess) falls at energies above 0.7 keV. The fact that energies below 0.7 keV are excluded in spectral fitting should therefore also reduce the problem. Finally, we do not see any systematic low-energy (~ 0.7–1 keV) residuals for any of the spectra. This suggests that systematic uncertainties in our background subtraction is not a major issue at low energies either.

5 COMBINING THE RESULTS

A radial profile of some quantity may not always provide a useful description for an individual system due to departures from spherical symmetry. The average of many such profiles derived for different groups should be much less affected though. Since our radial measurements for individual groups are statistically independent (as they are based on projected profiles), it is possible to explore general trends in the radial distributions of T and Z by superposing and averaging the profiles derived for individual groups. With the robustness of our results well established, we can therefore proceed to discuss these in a statistical framework on the basis of correlation tests and orthogonal regression analyses (Isobe et al. 1990) performed on the combined measurements. Throughout the section, we have used the Kendall rank-order correlation coefficient τ (in the range $[-1; +1]$, with $+1$ for a strong, positive correlation), and the associated significance σ_K of τ being non-zero, to quantify the strength and nature of any linear relationship between various quantities.

5.1 Temperature profiles

In order to examine the overall radial behaviour of T for our sample, we plot in Fig. 6 all temperature measurements, normalized to the mean temperature $\langle T \rangle$ of each group. In the plot, we have subdivided the data points according to whether they are inside or outside the T-peak located at $r(T_{\max})$, resulting in 134 and 58 measurements, respectively. For NGC 4125, which has a monotonically decreasing $T(r)$, we have grouped the data points inside D_{25} with those at $r < r(T_{\max})$. As discussed, temperature variations clearly exhibit a very similar overall behaviour. Similar to the case for clusters (e.g. Vikhlinin et al. 2005; Pratt et al. 2007), and as discussed quantitatively below, there is a clear indication that the intrinsic scatter in $T/\langle T \rangle$ is larger in the central regions, inwards of the temperature peak. This is not surprising, as non-gravitational processes other than radiative cooling could be important in this region, thus helping to break any self-similarity otherwise induced by gravity.

At first glance, Figure 6 appears to be suggestive of a bimodality in $T(r)$ in the core regions, but this could be largely driven by NGC 5044, which is better sampled than the other groups and displays lower central values of $T/\langle T \rangle$ than the majority. To investigate this in more detail, we tested for any evidence of bimodality in $T/\langle T \rangle$ by extracting the value for each group around a specific overdensity radius inside the cool core, excluding the non-cool core system NGC 4125. For $r \approx 0.01 r_{500}$, the smallest radius shown in Fig. 6, a Kolmogorov-Smirnov test indicates a 65 per cent probability that the resulting values have been drawn from a single Gaussian distribution with the given mean and variance. At $0.03 r_{500}$, however, there is some evidence for bimodality (see inset in Fig. 6), with the corresponding probability being only 12 per cent, but increasing again to 45 and 91 per cent at 0.05 and $0.07 r_{500}$, respectively. Intriguingly, we conclude that there is some evidence for a

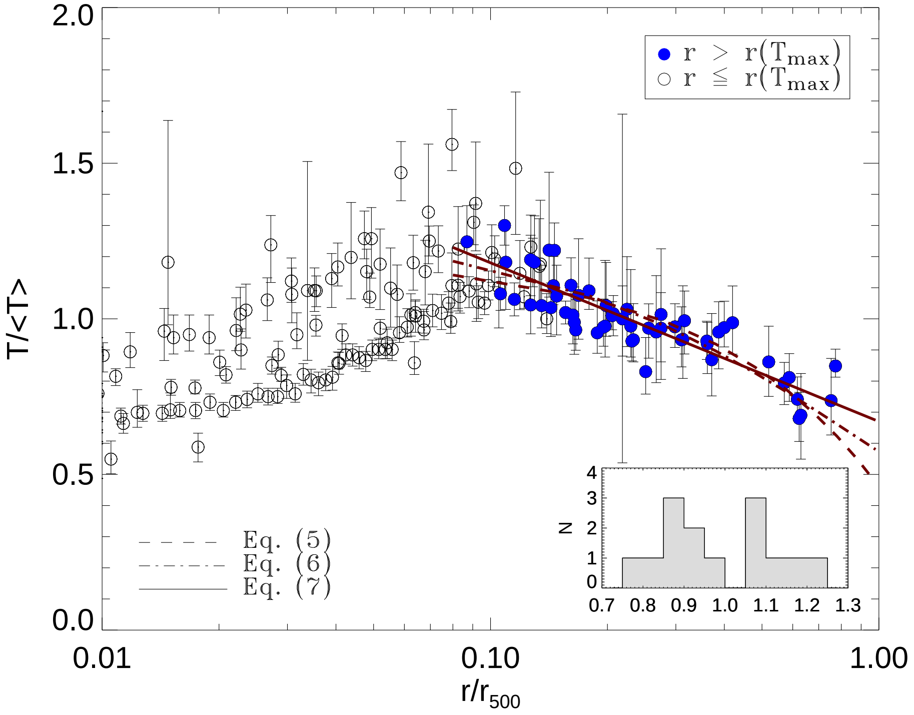

Figure 6. Temperature profiles of all groups, normalized to the mean temperature $\langle T\rangle$ of each group. Filled circles represent data points outside the position $r(T_{\rm max})$ of the temperature peak (i.e. outside the cool core), empty circles those inside. Lines show results of regression fits to the data, assuming various functional forms of $T/\langle T\rangle$ vs. r as described in equations (5)–(7). Inset shows the histogram of $T/\langle T\rangle$ at $r \approx 0.03r_{500}$ for the 14 cool-core groups.

bimodal $T/\langle T\rangle$ distribution around $r \approx 0.03r_{500}$, but the result is marginal in the sense that a unimodal Gaussian distribution cannot be rejected at 90 per cent confidence, in part due to the relatively small sample size. There is also no strong indications of bimodality at significantly smaller or larger radii.

In order to investigate the potential role of AGN feedback in establishing this tentative bimodality, we searched for a central radio source in the brightest group galaxy following the procedure outlined in Croston et al. (2005). Such a source was clearly identified in 11 of the groups (with the off-centre source in NGC 4125 as an additional candidate), and with HCG 42, MKW 4, and NGC 4325 as the only clear exceptions. For these 11 groups, testing for a linear correlation between $T/\langle T\rangle$ at $r \approx 0.03r_{500}$ and the 1.4 GHz power of this central radio source yields a value of Kendall's $\tau = +0.31$ and an associated significance of $\sigma_K = +1.3$. Thus, there is marginal statistical evidence for a correlation, but this is largely driven by the two most powerful sources (in NGC 383 and NGC 741), without which any correlation is absent ($\sigma_K = +0.4$). In conclusion, there appears to be no clear connection between this potential $T(r)$ bimodality and the current radio output of a central AGN. A larger sample would be useful for a more decisive test of the presence of a bimodality, and for addressing its possible origin.

It is also worth noting that we are probing the cores of these groups down to much smaller fractions of r_{500} than in typical cluster studies. Interestingly, excluding the non–cool core system NGC 4125, the ratio $T_c/\langle T\rangle$ of the temperature T_c in the innermost radial bin to the mean temperature $\langle T\rangle$ shows a mean and standard deviation of 0.58 and 0.14, respectively (0.61 and 0.17 if NGC 4125 is included). This is higher than the typical cool-core cluster value of $T_c/\langle T\rangle \approx 0.4$ found, for example, for the projected T-profiles of Vikhlinin et al. (2005) or the deprojected ones of Piffaretti et al. (2005) and Sanderson et al. (2006). It may reflect the fact that the temperature profiles of our groups flatten off at small radii (inside $r \approx 0.01r_{500}$), as suggested in Section 3.1, in contrast to what is seen in clusters. Fig. 5 indicates that deprojecting our profiles would not change this conclusion, as already suggested by the internal consistency among projected and deprojected cluster results.

An orthogonal regression fit to the temperature profiles inside the cool core – excluding the innermost $r < 0.01r_{500}$ because of the putative flattening in this region – yields

$$\log T/\langle T\rangle = (+0.21 \pm 0.02)\,\log(r/r_{500}) + (0.28 \pm 0.03). \quad (3)$$

The derived logarithmic slope of the profile in the core of ≈ 0.2 is in excellent agreement with the value of 0.23 ± 0.04 seen for groups in the radio-quiet (1.4 GHz radio power of central early-type $L < 10^{22}$ W Hz^{-1}) subsample of Jetha et al. (2007). It is, however, somewhat flatter than the slope of 0.34 ± 0.04 seen for their radio-loud subsample, or that of ≈ 0.4 found for clusters by Sanderson et al. (2006).

Hence, not only do the temperature profiles appear to flatten off in the very core of these groups, their rise with radius is also somewhat shallower than in clusters. We investigate these results from a slightly different perspective in Figure 7, plotting the ratio of T_c to the peak temperature $T_{\rm max}$ for each group. While this ratio is subject to considerable scatter at a given mean system temperature $\langle T\rangle$, there is a weak indication ($\tau = -0.43$, $\sigma_K = -1.3$) of a negative correlation between the quantities plotted (the low-lying

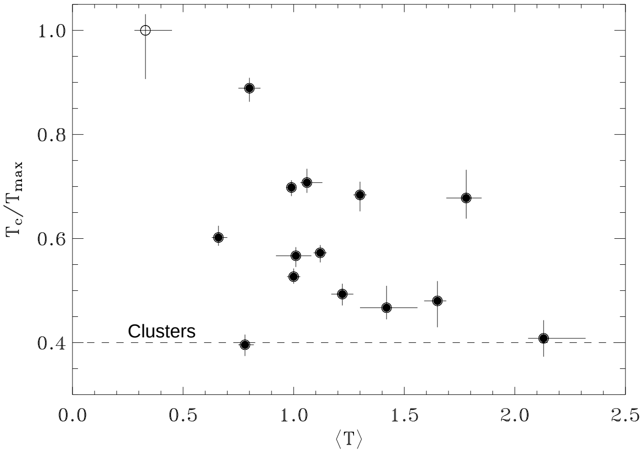

Figure 7. Ratio of core to peak temperature as a function of mean group temperature $\langle T\rangle$. NGC 4125, which has no cool core, is shown as an empty circle. Dashed line shows the typical cluster value of $T_c/T_{\rm max} \approx 0.4$ (e.g., Sanderson et al. 2006).

outlier in Fig. 7 is NGC 2300; if one were to exclude this data point, the significance of the correlation would increase to 2.2σ), thus confirming the notion that the cool core is less pronounced in groups than in clusters. The implication seems to be that, relative to the maximum temperature of the system, cooling in clusters can generally progress further than in groups, and this group–cluster discrepancy becomes increasingly pronounced towards lower mean system temperatures $\langle T\rangle$.

A potentially related issue is the radial extent of the cool cores. As mentioned in Section 3.1, the position $r(T_{\rm max})$ of the temperature peak varies slightly among the groups. In order to investigate whether this might reflect the properties of the central galaxy or the group itself, we plot in Fig. 8 $r(T_{\rm max})$ as a function of the size and mass (measured by D_{25} and L_K, respectively) of the central galaxy and of the mass of the group (measured by r_{500}), with K-band luminosities L_K taken from 2MASS (Skrutskie et al. 2006). Testing for a linear correlation between $r(T_{\rm max})$ and the three quantities plotted, we find $\tau = 0.62$ and $\sigma_K = 3.2$, for $r(T_{\rm max})$ vs. r_{500}. The corresponding significances for a correlation with L_K and D_{25} are 2.8 and 2.5σ, respectively. Although not a strong result, it suggests that the central temperature structure of the group is more closely related to the properties of the group as a whole than to those of the central galaxy (any correlation with central galaxy properties might naturally arise because D_{25} and L_K are themselves correlated with r_{500} at 2.5 and 2.7σ significance, respectively). Such an interpretation would be in qualitative agreement with the conclusions of Helsdon et al. (2001) and Helsdon & Ponman (2003) who found that the X-ray properties of gas surrounding central group galaxies are different from those of non-central galaxies and, indeed, appear more closely related to the group than to the central galaxy itself.

Even when excluding NGC 4125, by far the coolest group in our sample, a fit to the data in Fig. 8c gives the relation

$$r(T_{\rm max}) = (0.20 \pm 0.02)(r_{500}/{\rm kpc}) - (46.7 \pm 15.1)\ {\rm kpc}, \qquad (4)$$

which, perhaps coincidentally, would predict the observed absence of a cool core in NGC 4125. If this relation can indeed be extended to $r_{500} \lesssim 350$ kpc, the implication would be that systems with $r_{500} \lesssim 250$ kpc, or, more precisely, with $T \lesssim 0.3$ keV from equation (1), would generally not have cool cores. This is perhaps not surprising, as the central gas properties in systems of such low temperatures could be strongly affected by galactic feedback. Measured relative to r_{500}, Fig. 8c also shows that while the cool core is generally smaller than in clusters, it approaches the typical cluster extent at the high end of the temperature range covered by our sample, with group and cluster results becoming statistically indistinguishable at $T \gtrsim 2$ keV according to equations (1) and (4).

Outside the cool core, the temperature profiles in Fig. 6 clearly decline with r, appearing to drop by almost a factor of two out to r_{500}. A correlation test on the quantities plotted in Fig. 6 establishes a strong anticorrelation beyond $r = r(T_{\rm max})$, with $\tau = -0.70$ and $\sigma_K = -7.7$. For the data in this region, we attempted three different parametrizations for this decline of the T-profile. From a *Chandra* analysis of the projected temperature profiles of a sample of 13 massive, relaxed clusters (T-range 1–9 keV), Vikhlinin et al. (2005) find a relation $T/\langle T\rangle = -0.76 r/r_{500} + 1.22$ outside the cool core (assuming $r_{500} \approx 0.63 r_{180}$). A similar linear fit for our groups yields

$$T/\langle T\rangle = (-0.74 \pm 0.09)(r/r_{500}) + (1.20 \pm 0.02), \qquad (5)$$

for a reduced $\chi^2_\nu = 1.97$. Taken at face value, this relation, shown as a dashed line in Fig. 6, is in excellent agreement with that of the Vikhlinin et al. clusters, suggesting that temperature variations within groups are very similar to those of clusters at large radii, contrary to the case in the core. The resulting fit quality is poor, however, so a relation of the form of equation (5) is not particularly successful in describing our group data. The main reason is that such a parametrization cannot match the group data immediately outside the cool core without overpredicting observed temperatures at intermediate radii and underpredicting them further out.

As a possible alternative, we note that cosmological hydrodynamical simulations invoking gravity only have suggested a ‘universal’ temperature profile for massive ($T \gtrsim 3$ keV) clusters, of the form $T \propto (1 + 0.75 r/r_{500})^{-1.6}$ (Loken et al. 2002), assuming $r_{500} \approx 0.5 r_{100}$. This parametrization was shown by Loken et al. (2002) to be in good agreement with cluster results outside the core region, remaining a good description also when including galactic feedback and radiative cooling in the simulations. Motivated by this, we fitted a similar relation to our group data, yielding

$$T/\langle T\rangle = (1.29 \pm 0.03)(1 + 0.75 r/r_{500})^{-1.45 \pm 0.14} \qquad (6)$$

for $\chi^2_\nu = 1.65$. While resulting in a better fit than equation (5), this relation suffers from the same shortcomings in describing our data, albeit to a lesser degree. Nominally, the result, represented by a dash-dotted line in Fig. 6, is broadly consistent with that found for the simulated clusters of Loken et al. (2002), including the normalization factor of 1.33 found by the latter authors.

Prompted by the appearance of the data in Fig. 6, a third parametrization of the profiles was also investigated, in which T is a linear function of log (r/r_{500}). The fit result,

$$T/\langle T\rangle = (-0.51 \pm 0.04)\ \log(r/r_{500}) + (0.67 \pm 0.03), \qquad (7)$$

is statistically better ($\chi^2_\nu = 1.26$) than the results of equation (5) and (6). The intrinsic scatter about this relation is negligible, whereas the corresponding scatter around equation (3) is 12 per cent, thus confirming the indication of Fig. 6 that intrinsic scatter is larger in the core regions. The derived relation of equation (7) is plotted as a solid line in Fig. 6. The fact that equations (5) and (6) are good descriptions of both observed and simulated clusters, but are less representative of groups than equation (7), does not necessarily suggest the presence of intrinsic differences in the

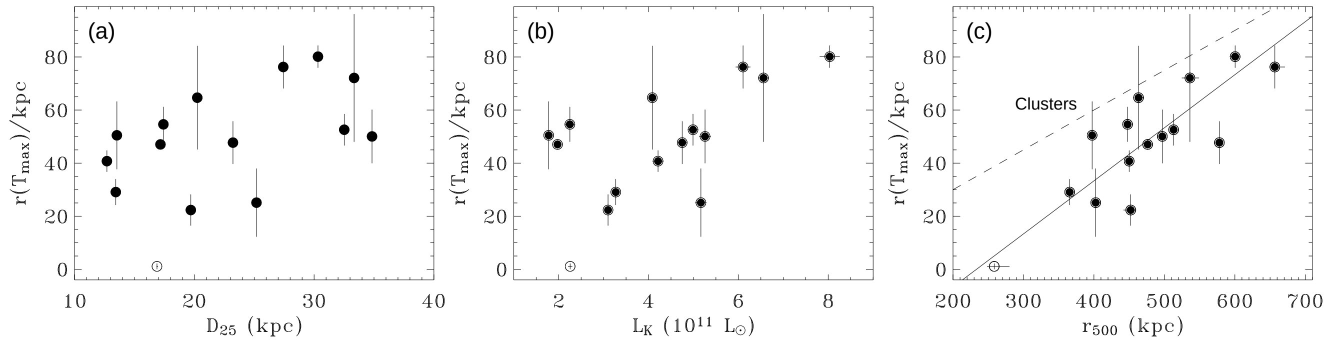

Figure 8. Radius $r(T_{\max})$ of maximum gas temperature as a function of (a) D_{25} of the central galaxy, (b) extinction-corrected K-band luminosity L_K of the central galaxy, and (c) r_{500} of the group. As in Fig. 7, NGC 4125 is represented by an empty circle. The solid line in Fig. 8c (with slope = 0.2) represents the best fit to the data excluding NGC 4125, while the dashed line shows the typical cluster result of $r(T_{\max}) \approx 0.15 r_{500}$ (e.g., Vikhlinin et al. 2005).

large-scale temperature structure of hot gas in these systems. The formal agreement with cluster results in terms of best-fitting parameters clearly indicate that the temperature profiles of cool-core groups at large radii are similar to those of clusters. We do not expect this conclusion to be affected by projection effects to an appreciable degree. Finally, we note that there is no indication that the possible bimodality in $T/\langle T\rangle$ at $r \approx 0.03 r_{500}$ is reflected in significantly different slopes at large r; assuming again a prescription of the form of equation (7) outside $r(T_{\max})$, we find consistent slopes of -0.49 ± 0.07 and -0.54 ± 0.04 for the low- and high-$T/\langle T\rangle$ subsamples seen in the inset of Fig. 6, respectively.

Summarizing, we find that cool cores in groups are less pronounced than those of clusters, in terms of both their spatial extent and relative temperature variation. At large radii, however, the temperature profiles of our groups decline with radius in consistency with results for more massive systems.

5.2 Iron and silicon profiles

In Fig. 9, all measurements of $Z_{\rm Fe}$ and $Z_{\rm Si}$ have been combined, demonstrating more clearly the central excess in iron abundance and the general decrease to a value of ~ 0.1 Z$_\odot$ at large radii suggested by Fig. 3. For $Z_{\rm Fe}$, there appears to be a clear trend with radius outside the cool core, and a test performed on the data points outside $r(T_{\max})$ confirms the presence of a linear correlation between log $Z_{\rm Fe}$ and log (r/r_{500}) at the 5.1σ level ($\tau = -0.46$). Inside the core, the data are consistent with a constant Fe abundance ($\sigma_K = 0.0$), but this may mask a more complex behaviour as discussed below.

The Si profiles are fairly similar to those of Fe in the group cores, showing no systematic trend with radius ($\sigma_K = -0.1$). Si also appears from Fig. 9 to show less systematic radial variation outside the core than Fe. Indeed, outside $r(T_{\max})$ no significant correlation ($\tau = -0.07$, $\sigma_K = -0.8$) is found between log $Z_{\rm Si}$ and log (r/r_{500}), though the value of τ suggests a mild overall decline with radius. The situation is qualitatively similar to that seen for clusters, where Si generally shows a more uniform distribution than Fe (Finoguenov et al. 2000). As is evident from Fig. 3, $Z_{\rm Si}$ actually rises with radius in the outskirts for some of the groups, a fact which clearly contributes to obscuring any statistical evidence for a simple linear behaviour. A similar feature has been noted in some relatively cool clusters but is seemingly absent in hotter systems (Finoguenov et al. 2000, 2001a).

In addition to the considerable statistical errors on the derived abundance data, particularly for Si at large radii, there is clearly also substantial intrinsic scatter among the groups at any given radius. Coupled with the lack of a clear radial correlation for Si, we have consequently refrained from fitting regression lines to the raw data in Fig. 9a. In an attempt to suppress these intrinsic variations, we also plot in Fig. 9b the abundance data normalized to the mean value $\langle Z\rangle$. As suggested by the figure, the resulting correlation is slightly stronger for $Z_{\rm Fe}$ ($\tau = -0.61$, $\sigma_K = -6.8$) but is still not very significant for Si ($\sigma_K = -1.2$). The latter result is perhaps not surprising, given that the normalization factor, i.e. the mean abundance $\langle Z\rangle$, has been derived assuming all abundances fixed relative to solar, so the fitted value of $\langle Z\rangle$ will be driven by the abundance as estimated from the prominent Fe lines.

5.3 The silicon-to-iron ratio $Z_{\rm Si}/Z_{\rm Fe}$

The strong radial decline of $Z_{\rm Fe}$ and the hint of a more gentle decline of $Z_{\rm Si}$ are also reflected in an increase in $Z_{\rm Si}/Z_{\rm Fe}$ at large radii, as illustrated in Fig. 10. This figure further suggests the presence of a dichotomy in the radial distribution of $Z_{\rm Si}/Z_{\rm Fe}$, with this quantity being roughly constant inside $r(T_{\max})$ but rising further out. A correlation test confirms that within the cool core there is only marginal evidence for a systematic variation in this quantity ($\tau = 0.08$, $\sigma_K = 1.3$), suggesting a mild radial decrease, with the data showing a mean and 1σ dispersion pf 0.91 ± 0.29 Z$_{\rm Si,\odot}$/Z$_{\rm Fe,\odot}$. This mean value is thus slightly lower than, but consistent with, the local (Solar neighbourhood) IMF and SN mixture. For the adopted SN yields, the value corresponds to a mixture of 70 per cent core-collapse SN and 30 per cent SN Ia by number, in excellent agreement with recent results for the cores of clusters (see de Plaa et al. 2007 and references therein), and consistent with the observed proportion of SN types at low redshift ($z \lesssim 0.5$) determined from the *Hubble* and *Chandra* Deep Fields (Dahlen et al. 2004). For the adopted SN yields, this implies that SN Ia are the dominant Fe contributor in group cores, being responsible for 79 ± 13 per cent of the Fe in this region. This agrees not only with results for cluster cores, as mentioned, but is also in accord with the corresponding fraction for the hot gas in elliptical galaxies of 66 ± 11 per cent (Humphrey & Buote 2006).

Outside $r(T_{\max})$, the correlation test confirms that $Z_{\rm Si}/Z_{\rm Fe}$ rises with radius ($\tau = 0.21$, $\sigma_K = 2.3$), but the trend is probably suppressed due to large statistical scatter. We note that many of the data points with very low $Z_{\rm Si}/Z_{\rm Fe}$ have $Z_{\rm Si} \approx 0$ rather than high $Z_{\rm Fe}$, but these have large fractional errors and most are consistent

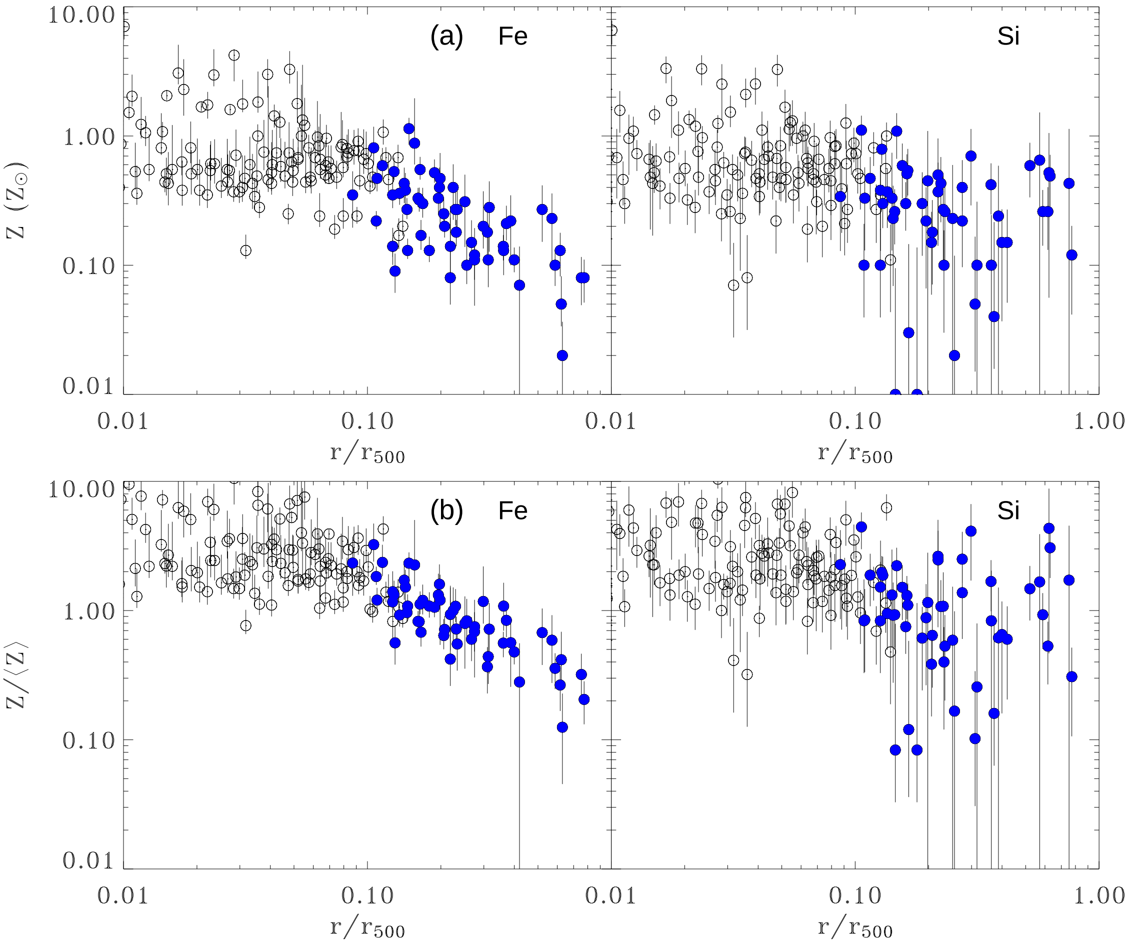

Figure 9. (a) $Z_{\rm Fe}$ and $Z_{\rm Si}$, all measurements. Symbols are as in Fig. 6. (b) The same data normalized to $\langle Z \rangle$.

with the general trend. Similar to the case for clusters and as further illustrated in Fig. 10b, the high central Fe abundance seen in most of our systems can thus be ascribed predominantly to SN Ia, with an increasing SN II contribution towards larger radii and lower Fe abundances. We also note that the global mean and standard deviation of $Z_{\rm Si}/Z_{\rm Fe}$, derived from those data points for which the fractional errors (at 90 per cent confidence) on both $Z_{\rm Si}$ and $Z_{\rm Fe}$ are less than 100 per cent, are ≈ 1.3 and 0.8 in solar units, respectively, in agreement with the (radially constant) ratio of 1.4 ± 0.2 found for the $T < 6$ keV subsample of Tamura et al. (2004). The fact that our groups do *not* show a radially constant ratio is reflected in a large standard deviation around the global mean.

5.4 Binning the profiles

To better investigate radial trends and further suppress intrinsic scatter among the groups, we plot profiles of all data points in Fig. 11, accumulated in radial bins of 20 measurements. In this representation, the temperature profiles are clearly seen in Fig. 11a to peak at a radius $r \approx 0.1r_{500}$, while flattening out in the group cores. We re-iterate that this central flattening is not observed in clusters, even in cases where the cluster cores are well resolved on scales below $0.01r_{500}$ (e.g., Sanderson et al. 2006).

For the Fe abundance, Fig. 11b reveals roughly solar abundances in the group cores, consistent with the results found for X-ray bright ellipticals by Humphrey & Buote (2006), five of which constitute the central group elliptical in our sample. The figure also confirms the trends discussed above, indicating that outside the core, $Z_{\rm Fe}$ continuously declines out to the largest measured radii. The binned results further enable a straightforward comparison to the corresponding Fe profile found for cool-core clusters by De Grandi et al. (2004). This reveals similar values of Fe enrichment within the central abundance excess in groups and clusters ($Z_{\rm Fe} \approx 0.8$ Z$_\odot$), with some indication that the excess is slightly broader in clusters; our binned Fe profile declines from its central value by a factor of two around $r \approx 0.2r_{500}$, whereas the corresponding radius for the De Grandi et al. (2004) clusters is $r \approx 0.3r_{500}$. The De Grandi et al. (2004) clusters display a flattening in the Fe profile beyond $0.3r_{500}$. contrary to what is observed for our groups. Note also that the off-centre abundance peaks hinted at in many of the groups with well-resolved cores, and the considerable intrinsic scatter these peaks cause in this representation, are visible for both the binned Fe and Si profiles, even when these are normalized to the mean abundances.

The binning of the abundance profiles clearly suppresses the considerable scatter seen in Fig. 9, resulting in a much more well-defined radial behaviour for both Fe and Si. We performed linear regression fits to these sample-averaged profiles in order to characterize the reasonably uniform behaviour outside the very group

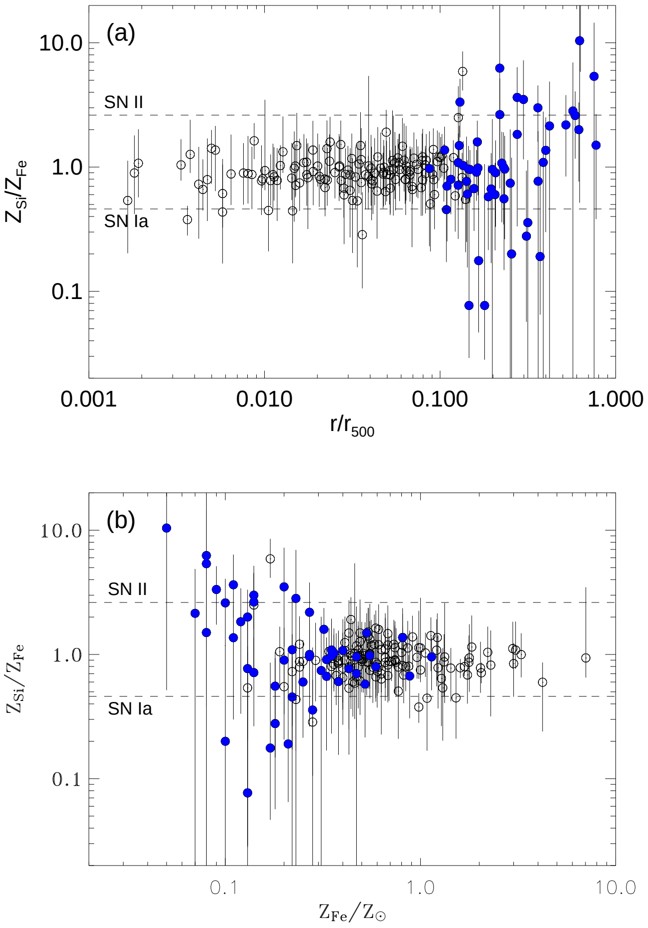

Figure 10. $Z_{\rm Si}/Z_{\rm Fe}$, all measurements, in units of the Solar ratio and as a function of (a) radius and (b) $Z_{\rm Fe}$ (with error bars on $Z_{\rm Fe}$ omitted for clarity). Symbols are as in Fig. 6. Dashed lines mark the ratios expected from pure SN Ia and SN II enrichment, as in Fig. 4.

cores. Excluding the innermost data point in Fig. 11b, orthogonal regression on the binned Fe profile yields

$$\log Z_{\rm Fe} = (-0.66 \pm 0.05) \log(r/r_{500}) - (1.00 \pm 0.06) \qquad (8)$$

relative to the corresponding solar abundances. The Fe abundance at r_{500} suggested by this relation of $Z_{\rm Fe} \simeq 0.1$ Z$_\odot$ is lower than the typical value of ~ 0.2 Z$_\odot$ seen in the outskirts (at $r \approx r_{500}$) of clusters (e.g., Finoguenov et al. 2000; De Grandi & Molendi 2001; Tamura et al. 2004). This is particularly true in light of the fact that we have adopted the abundance table of Grevesse & Sauval (1998), for which the Solar Fe abundance is only 68 per cent of the Anders & Grevesse (1989) value typically used in previous cluster studies. The Fe abundance in those previous studies must therefore be multiplied by 1.48 for a direct comparison to our results (the Si abundance, on the other hand, remains unaffected to within 1 per cent by this change in abundance table).

Fig.11c suggests that $Z_{\rm Si}$ also declines outside the cool core, despite the fact that there is only marginal statistical evidence for a radial decline of $Z_{\rm Si}$ outside $r(T_{\rm max})$ in the unbinned data. As already indicated by the dichotomy in the Si/Fe ratio (Fig. 10), the reason for this apparent inconsistency is that while Si does decline immediately outside the cool core, it flattens out or even rises at the largest radii probed, thus suppressing any statistical evidence for a uniformly declining profile outside the core. Beyond $0.4r_{500}$, roughly corresponding to the range covered by the outermost data point in Fig. 11c, the unbinned Si data show no clear correlation with r ($\sigma_K = -0.7$). To capture this behaviour, we performed a regression fit to all but the innermost data point in Fig.11c, and assumed $Z_{\rm Si}(r)$ to remain constant beyond the outermost data point at $r \approx 0.5r_{500}$, yielding

$$\log Z_{\rm Si} = \begin{cases} m \log(r/r_{500}) + c, & r \leqslant 0.5r_{500} \\ 0.25 \pm 0.05 \ {\rm Z}_\odot \quad , & r > 0.5r_{500} \end{cases} , \qquad (9)$$

with $m = -0.44 \pm 0.07$ and $c = -0.74 \pm 0.06$. The value of 0.25 Z$_\odot$ at $r > 0.5r_{500}$ was chosen to ensure continuity, with its errors based on the fractional errors on the outermost data point. An Si abundance of $\sim$ 0.2–0.25 Z$_\odot$ at r_{500} is also in good agreement with earlier *ASCA* results for groups (Finoguenov et al. 2002), whereas clusters tend to show slightly higher values of $\sim$ 0.3–0.5 Z$_\odot$ (Finoguenov et al. 2000, 2001a) at large radii. This suggests a higher content of *both* Fe and Si in the outskirts of more massive systems. However, a direct comparison is somewhat impeded by the large statistical uncertainties on $Z_{\rm Si}$ in groups, as well as the fact that $Z_{\rm Si}(r)$ does not show a uniform behaviour at large r across our sample.

For the $Z_{\rm Si}/Z_{\rm Fe}$ ratio, a subsolar value is seen in the innermost bin in Fig. 11f, with the ratio rising to ≈ 1 within $0.1r_{500}$ and further to $\gtrsim 2$ well outside the central galaxy. As discussed in Section 4, we believe that the result for the outermost bin is not seriously affected by uncertainties in our background subtraction. The result demonstrates more clearly what was already indicated by Fig. 10, that SN Ia provide a dominant, but not exclusive, contribution to the enrichment within the cool core and hence inside the optical extent of the central galaxy. Well outside the group core the dominant contribution comes from SN II, and at large radii the $Z_{\rm Si}/Z_{\rm Fe}$ ratio rises to become consistent with the value of ≈ 2.6 expected for pure SN II enrichment. Corrected for differences in adopted abundance tables, the value of the outermost bin in Fig. 11f is at least as high those of the Finoguenov et al. (2000) clusters. Our results, therefore, do not support the claim of the latter authors that groups on average have lower Si/Fe ratios at large radii than clusters. The results further indicate that, on average, both SN Ia and SN II enrichment is required at all radii within at least $r \approx 0.5r_{500}$. While this relies on the assumption that derived abundances in the central region are not seriously affected by the Fe and Si biases, similar central $Z_{\rm Si}/Z_{\rm Fe}$ ratios of $\gtrsim 1$ have also been found in *ASCA* and *XMM* observations of hotter clusters (Finoguenov et al. 2000; Tamura et al. 2004), although it should be mentioned that the cores of these clusters are generally less well resolved than those of our groups.

Summarizing, we find that the distributions of both Fe and Si in the unbinned data (Fig. 9) appear roughly uniform in the group cores, but the averaged profiles clearly confirm the evidence for off-centre peaks in some of the groups. The enrichment in the cores contain a significant contribution from SN Ia, probably hosted by the central, bright galaxy, an issue to which we will return in Paper II. On average, SN II dominate by *number* at all radii, in agreement with the results obtained by Finoguenov & Ponman (1999) for a sample of three groups, and can on their own explain the observed abundances well outside the group core. We believe this latter conclusion to be reasonably robust with respect to any remaining background issues. A high Si/Fe ratio consistent with, or even exceeding, the expectation from our adopted SN II yields is seen in the outermost bin of *all* of our groups, including groups such as NGC 383, HCG 62, and NGC 5044, for which the data feature

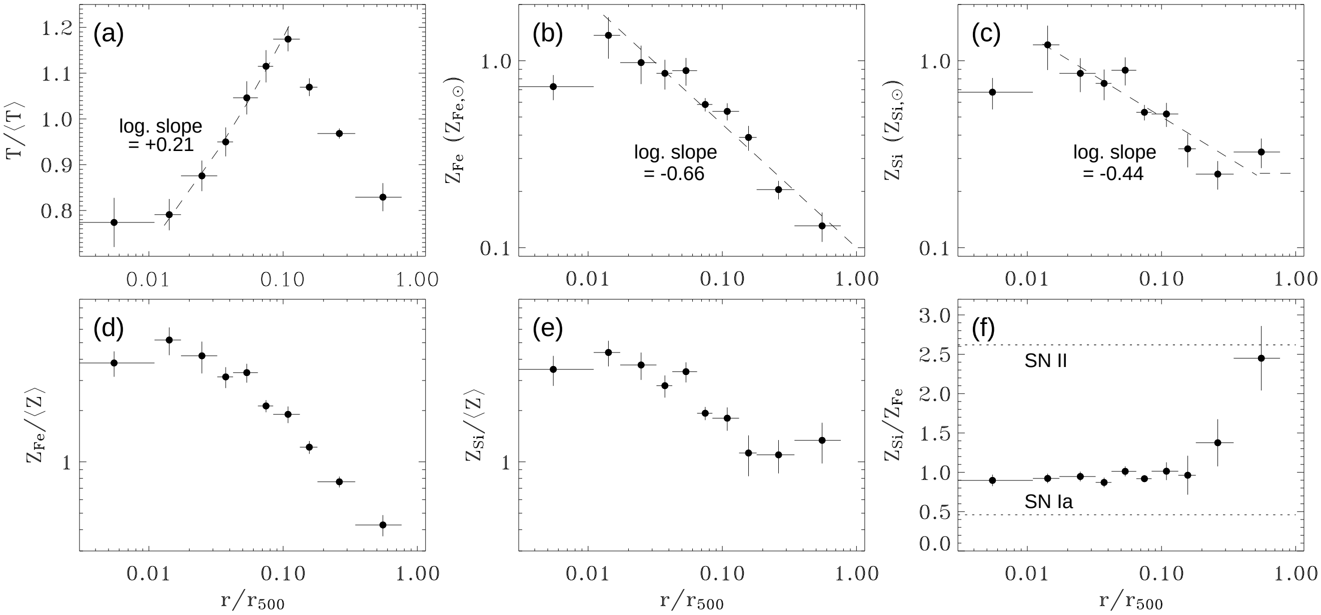

Figure 11. Profiles for all groups, binned into radial bins of $N = 20$ data points. Errors represent the standard deviation in each bin divided by $\sqrt{N}$. Dashed lines in (a)–(c) mark the best-fitting regression lines across the radial ranges shown, i.e. equations (3), (8), and (9).

high signal-to-noise ratios even at large radii. Support for this result comes from the work of Finoguenov et al. (2000), in which a rise in $Z_{\rm Si}/Z_{\rm Fe}$ to supersolar values at large radii is also seen for the groups in their sample. The trend of Si/Fe increasing with radius has also been reproduced in cosmological simulations in which the galactic feedback implementation favours the ejection of SN II products over those of SN Ia (Romeo et al. 2006).

We note that the interpretation that SN II alone can explain the observed abundance pattern at large radii is reasonably robust to the choice of theoretical SN II yields available in the literature. For example, for a standard Salpeter IMF, none of the SN II model yields considered by Gibson et al. (1997) would predict $Z_{\rm Si}/Z_{\rm Fe} > 2.6$. Hence our conclusion regarding the SN II contribution is only compromised if invoking a more ‘top-heavy’ IMF, with $x < 1.0$ in equation (2). In connection with this, it is worth pointing out, on the basis of the outermost three data points of Fig. 11f, that the slope of $Z(r)$ for at least one of the two elements must change beyond r_{500} if the observed Si/Fe ratio is to remain consistent with the IMF and SN model yields adopted here. Deep, high–S/N X-ray observations of group outskirts could shed light on this issue and thus help constrain theoretical SN yields, but such a study could well be beyond the capabilities of current X-ray telescopes for all reasonable exposure times. With their higher X-ray surface brightness at large radii, cool to intermediate-temperature clusters ($T \approx 2 - 4$ keV) remain more attractive targets for this purpose, also because they show prominent emission lines from a wider range of relevant elements (e.g., Finoguenov et al. 2000, 2001a).

6 SUMMARY AND CONCLUSIONS

We have conducted a homogeneous analysis of a sample of 15 X-ray bright galaxy groups observed by *Chandra*, selected for their relatively undisturbed X-ray morphology and good photon statistics. Correlation tests and regression fits have been performed on the combined radial temperature and abundance profiles and derived quantities, both to investigate the nature of any relationship between various quantities, and to enable straightforward comparison to results of numerical simulations of group formation and evolution.

Our derived radial temperature profiles show remarkable similarity when scaled to the mean system temperature $\langle T \rangle$ derived outside the central region, and reveal that all but one group show clear evidence for a cool core. We find that these cores are smaller than those seen in clusters, both in absolute physical extent and relative to a fixed overdensity radius, and that their sizes appear more closely related to the properties of the group as a whole than to those of the central early-type galaxy present in all our groups. The absolute and relative cool core sizes approach those of clusters at the high–temperature end of our sample. The temperature profiles in the core are also shallower than those seen in clusters, equivalent to a less pronounced temperature decline in the core relative to the peak temperature displayed by the system. This may indicate that radiative cooling can generally progress further in more massive systems. The flatter group profiles inwards of the temperature peak relative to those of more massive systems certainly point to clear differences in the central ICM heating history among systems of varying mass. We find tentative evidence for a bimodality in $T/\langle T \rangle$ inside the cool core, but this is confined to a narrow interval in radius and is not mirrored by differing slopes in the temperature profiles at large radii, which we find to be similar to those found for both observed and simulated clusters.

The Fe and Si abundance profiles show a number of distinct features common to most of the groups. Similar to the case for cool-core clusters, a central enhancement in Fe abundance is clearly seen in all but two groups, one of which is NGC 4125, the only non–cool core group in our sample. This Fe excess can extend well beyond the optical extent of the central early-type galaxy present in all groups, and is in many cases accompanied by a similar feature in the Si distribution. In many of the groups with a well-resolved core, evidence for an off-centre abundance peak is also observed inside the central galaxy, with a decline in abundance at the very centre, similar to results for some well-resolved cluster cores. Outside the central excess, the Fe profiles generally show a steep decline, approaching a value of $Z_{\mathrm{Fe}} \approx 0.1$ solar at r_{500}. This is lower than the corresponding typical cluster value by a factor of two, suggesting fundamental differences in enrichment history for the outskirts of these low-mass systems compared to more massive clusters. Si shows similar overall features but declines less steeply with radius, and flattens out or even rises again at large radii for the majority of the groups. On average, Si reaches a value of $Z_{\mathrm{Si}} \approx 0.25 - 0.3$ solar at r_{500}, again slightly below typical cluster values.

For the adopted SN yields, the ratio of Si to Fe abundance in the groups reveals a clear predominance of SN Ia enrichment in the central regions, with 79 ± 13 per cent of the Fe originating in SN Ia. This is in line with results for both hot gas in elliptical galaxies and the cores of massive clusters, suggesting a very similar enrichment istory for the central regions in such systems across three orders of magnitude in total system mass. The SN II contribution in our groups increases with radius, however, and at the largest radii probed, or, equivalently, at the lowest Fe abundances, the Si/Fe ratio is close to, and nearly always consistent with, the expectation for pure SN II enrichment in all groups. We find no indication that Si/Fe ratios at large radii are significantly different from the corresponding values in clusters. We note, however, that the existence of two separate SN Ia populations, as suggested by Mannucci et al. (2006), could complicate the interpretation of these results.

The abundance distribution in the intragroup medium is expected to be tightly linked to the star formation history in groups. In a forthcoming companion paper, we decompose the derived abundance profiles into contributions from the two major supernova types to explore this issue, along with the implications of our results for supernova and ICM energetics, the role of AGN and mergers in redistributing and reheating the enriched gas, and more generally for the enrichment history of the groups.

ACKNOWLEDGMENTS

We thank Stephen Helsdon for his contribution to the early stages of this project. We are grateful to Alexis Finoguenov and John Osmond for useful discussions and for providing comparison data for their group samples prior to publication. This work has made use of the NASA/IPAC Extragalactic Database (NED) and the Two Micron All Sky Survey (2MASS) database. JR acknowledges the support of the European Community through a Marie Curie Intra-European Fellowship.

REFERENCES

Anders E., Grevesse N., 1989, Geochim. Cosmochim Acta, 53, 197

Arnaud M., Rothenflug R., Boulade O., Vigroux L., Vangioni-Flam E., 1992, A&A, 254, 49

Balestra I., Tozzi P., Ettori S., Rosati P., Borgani S., Mainieri V., Norman C., Viola M., 2007, A&A 462, 429

Baumgartner W.H., Loewenstein M., Horner D.J., Mushotzky R.F., 2005, ApJ, 620, 680

Böhringer H., Matsushita K., Churazov E., Finoguenov A., Ikebe Y., 2004, A&A, 416, L21

Buote D.A., 2000a, MNRAS, 311, 176

Buote D.A., 2000b, ApJ, 539, 172

Buote D.A., Lewis A.D., Brighenti F., Mathews W.G., 2003a, ApJ, 594, 741

Buote D.A., Lewis A.D., Brighenti F., Mathews W.G., 2003b, ApJ, 595, 151

Buote D.A., Brighenti F., Mathews W.G., 2004, ApJL, 607, L91

Condon J.J., Cotton W.D., Greisen E.W., Yin Q.F., Perley R.A., Taylor G.B., Broderick J.J., 1998, AJ, 115, 1693

Cora S.A., 2006, MNRAS, 368, 1540

Croston J.H., Hardcastle M.J., Birkinshaw M., 2005, MNRAS, 357, 279

Dahlen T., et al., 2004, ApJ, 613, 189

Davis D.S., Mulchaey J.S., Mushotzky R.F., Burstein D., 1996, ApJ, 460, 601

Davis D.S., Mulchaey J.S., Mushotzky R.F., 1999, ApJ, 511, 34

De Grandi S., Molendi S., 2001, ApJ, 551, 153

De Grandi S., Ettori S., Longhetti M., Molendi S., 2004, A&A, 419, 7

de Plaa J., Werner N., Bleeker J.A.M., Vink J., Kaastra J.S., Mendez M., 2007, A&A, 465, 345

Dickey J. M., Lockman F. J., 1990, ARA&A, 28, 215

Domainko W., et al., 2006, A&A, 452, 795

Donahue M., Horner D.J., Cavagnolo K.W., Voit G.M., 2006, ApJ, 643, 730

Edwards L.O.V., Hudson, M.J., Balogh M.L., Smith R.J., 2007, MNRAS, in press (arXiv:0704.3242)

Ettori S., Fabian A.C., 2006, MNRAS, 369, L42

Ettori S., Fabian A.C., Allen S.W., Johnstone R.M., 2002, MNRAS, 331, 635

Fabbiano G., Schweizer F., 1995, ApJ, 447, 572

Finoguenov A., Ponman T.J., 1999, MNRAS, 305, 325

Finoguenov A., David L.P., Ponman T.J., 2000, ApJ, 544, 188

Finoguenov A., Arnaud M., David L.P., 2001a, ApJ, 555, 191

Finoguenov A., Reiprich T.H., Böhringer H., 2001b, A&A, 368, 749

Finoguenov A., Jones C., Böhringer H., Ponman T.J., 2002, ApJ, 578, 74

Finoguenov A., Burkert A., Böhringer H., 2003, ApJ, 594, 136

Finoguenov A., Davis D.S., Zimer M., Mulchaey J.S., 2006, ApJ, 646, 143 (F06)

Finoguenov A., Ponman T.J, Osmond J.P.F., Zimer M., 2007, MNRAS, 374, 737 (F07)

Forbes D.A., Thomson R.C., 1992, MNRAS, 254, 723

Fukazawa Y., Kawano N., Kawashima K., 2004, ApJL, 606, L109

Fukazawa Y., Makishima K., Tamura T., Ezawa H., Xu H., Ikebe Y., Kikuchi K., Ohashi T., 1998, PASJ, 50, 187

Fukazawa Y., et al., 1996, PASJ, 48, 395

Gastaldello F., Buote D., Humphrey P., Zappacosta L., Bullock J., Brighenti F., Mathews W., 2005, in Proceedings of the The X-ray Universe 2005, A. Wilson, ed., ESA SP-604, p. 743

Gibson B.K., Loewenstein M., Mushotzky R.F., 1997, MNRAS, 290, 623

Gilfanov M.R., Sunyaev R.A., Churazov E.M., 1987, SvAL, 13, 3

Grevesse N., Sauval A.J., 1998, Space Sci. Rev., 85, 161

Helsdon S.F., Ponman T.J., 2003, MNRAS, 340, 485

Helsdon S.F., Ponman T.J., O'Sullivan E., Forbes D.A., 2001, MNRAS, 325, 693

Humphrey P.J., Buote D.A., 2006, ApJ, 639, 136

Hwang U., Mushotzky R.F., Burns J.O., Fukazawa Y., White R.A., 1999, ApJ, 516, 604

Irwin J.A., Bregman J.N., 2001, ApJ, 546, 150

Isobe T., Feigelson E.D., Akritas M.G., Babu G.J., 1990, ApJ, 364, 104

Iwamoto K., Brachwitz F., Nomoto K., Kishimoto N., Umeda H., Hix, W.R., Thielemann F.-K., 1999, ApJS, 125, 439

Jetha N.N., Ponman T.J., Hardcastle M.J., Croston J.H., 2007, MNRAS, 376, 193

Johnstone R.M., Allen S.W., Fabian A.C., Sanders J.S., 2002, MNRAS, 336, 299

Jones L.R., Ponman T.J., Horton A., Babul A., Ebeling H., Burke D.J., 2003, MNRAS, 343, 627

Kim D.-W., Fabbiano G., 2004, ApJ, 613, 933

Khosroshahi H.G., Jones L.R., Ponman T.J., 2004, MNRAS, 349, 1240

Kraft R.P., Forman W.R., Churazov E., Laslo N., Jones C., Markevitch M., Murray S.S., Vikhlinin A., 2004, ApJ, 601, 221

Laing R.A., Bridle A.H., 2002, MNRAS, 336, 1161

Loken C., Norman M.L., Nelson E., Burns J., Bryan G.L., Motl P., 2002, ApJ, 579, 571

McNamara B.R., Nulsen P.E.J., Wise M.W., Rafferty D.A., Carilli C., Sarazin C.L., Blanton E.L., 2005, Nature, 433, 45

Mannucci F., Della Valle M., Panagia N., 2006, MNRAS, 370, 773

Mathews W.G., Brighenti F., Buote D.A., Lewis A.D., 2003, ApJ, 596, 159

Moll R., et al., 2007, A&A, 463, 513

Morita U., Ishisaki Y., Yamasaki N.Y., Ota N., Kawano N., Fukazawa Y., Ohashi T., 2006, PASJ, 58, 719

Mulchaey J.S., Davis D.S., Mushotzky R.F., Burstein D., 2003, ApJS, 145, 39

Mushotzky R., Loewenstein M., Arnaud K.A., Tamura T., Fukazawa Y., Matsushita K., Kikuchi K., Hatsukade I., 1996, ApJ, 466, 686

Nomoto K., Tominaga N., Umeda H., Kobayashi C., Maeda K., 2006, Nucl. Phys. A, 777, 428

Osmond J. P. F., Ponman T. J., 2004, MNRAS, 350, 1511

Osmond J.P.F., Ponman T.J., Finoguenov A., 2004, MNRAS, 355, 11

O'Sullivan E., Vrtilek J.M., Read A.M., David L.P., Ponman T.J., 2003, MNRAS, 346, 525

O'Sullivan E., Vrtilek J.M., Kempner J.C., 2005, ApJL, 624, L77

O'Sullivan E., Vrtilek J.M., Harris D.E., Ponman T.J, 2007, ApJ, 658, 299

Piffaretti R., Jetzer P., Kaastra J.S., Tamura T., 2005, A&A, 433, 101

Pratt G.W., Böhringer H., Croston J.H., Arnaud M., Borgani S., Finoguenov A., Temple R.F., 2007, A&A, 461, 71

Rasmussen J., Ponman T.J., Mulchaey J.S., 2006, MNRAS, 370, 453

Rebusco P., Churazov E., Böhringer H., Forman W., 2006, MNRAS, 372, 1840

Roediger E., Brüggen M., Rebusco P., Böhringer H., Churazov E., 2007, MNRAS, 375, 15

Romeo A.D., Sommer-Larsen J., Portinari L., Antonuccio-Delogu V., 2006, MNRAS, 371, 548

Russell P.A., Ponman T.J., Sanderson A.J.R., 2007, MNRAS, in press (astro-ph/0703010)

Sanders J.S., Fabian A.C., 2002, MNRAS, 331, 273

Sanders J.S., Fabian A.C., Dunn R.J.H., 2005, MNRAS, 360, 133

Sanderson A.J.R., Ponman T.J., O'Sullivan E., 2006, MNRAS, 372, 1496

Skrutskie M.F., et al., 2006, AJ, 131, 1163.

Tamura T., Kaastra J.S., den Herder J.W.A., Bleeker J.A.M., Peterson J.R., 2004, A&A, 420, 135

Tornatore L., Borgani S., Matteucci F., Recchi S., Tozzi P., 2004, MNRAS, 349, L19

Tozzi P., Rosati P., Ettori S., Borgani S., Mainieri V., Norman C., 2003, ApJ, 593, 705

Trentham N., Tully R.B., Mahdavi A., 2006, MNRAS, 369, 1375

Vikhlinin A., Markevitch M., Murray S.S., Jones C., Forman W., Van Speybroeck L., 2005, ApJ, 628, 655

Vrtilek J.M., David L.P., Grego L., Jerius D., Jones C., Forman W., Donnelly R.H., Ponman T.J., 2000, in Durret F., Gerbal D., eds, Constructing the Universe with Clusters of Galaxies, l'Institut d'Astrophysique de Paris, Paris

Zhang Y.-Y., Böhringer H., Finoguenov A., Ikebe Y., Matsushita K., Schuecker P., Guzzo L., Collins C.A., 2006, A&A, 456, 55

This paper has been typeset from a TEX/ LATEX file prepared by the author.